CRISPR-mediated insertion of a chimeric antigen receptor produces nonviral T cell products capable of inducing solid tumor regression

Katherine P. Mueller[1,2,7], Nicole J. Piscopo[1,2,7], Matthew H. Forsberg[4], Louise A. Saraspe[1], Amritava Das[1,5], Brittany Russell[1], Madeline Smerchansky[1,2], Lei Shi[4], Adeela Ali[4], Cicera R. Lazzarotto[6], Shengdar Q. Tsai[6], Christian M. Capitini[3,4*], Krishanu Saha[1,2,3*]

1. Wisconsin Institute for Discovery, University of Wisconsin-Madison, Madison, Wisconsin USA
2. Department of Biomedical Engineering, University of Wisconsin-Madison, Madison, Wisconsin USA
3. University of Wisconsin Carbone Cancer Center, University of Wisconsin-Madison, Madison, Wisconsin USA
4. Department of Pediatrics, University of Wisconsin School of Medicine and Public Health, Madison, Wisconsin USA
5. Morgridge Institute for Research, University of Wisconsin-Madison, Madison, Wisconsin USA
6. Department of Hematology, St Jude Children's Research Hospital, Memphis, TN, USA
7. These authors contributed equally: Katherine P. Mueller and Nicole J. Piscopo

*email: ccapitini@pediatrics.wisc.edu; ksaha@wisc.edu

Keywords: cell manufacturing, cell therapy, gene editing, immunotherapy, biomanufacturing, GD2, neuroblastoma, somatic cell gene editing, CRISPR/Cas9, CAR T cells

Abstract

Chimeric antigen receptor (CAR) T cells traditionally harbor viral vectors that encode the CAR transgene in the genome. However, viral vector manufacturing typically is resource intensive, suffers from batch-to-batch variability, and includes several animal components, adding regulatory and supply chain pressures. Here, CAR T cells were generated within nine days using recombinant *Sp*Cas9 protein and nucleic acids, without any viral vectors or animal components. In comparison to traditional retroviral CAR T cells, nonviral CAR T cells exhibit *TRAC*-targeted genomic integration of the CAR transgene, gene expression signatures associated with a memory phenotype, and low receptor signaling prior to infusion. Upon exposure to the GD2 target antigen, the nonviral anti-GD2 CAR cells exhibited specific cytotoxicity against GD2+ cells *in vitro* and induced solid tumor regression *in vivo*, with robust homing and persistence within a murine neuroblastoma xenograft model. This proof-of-principle study eliminating viral vectors and animal components during CAR gene transfer could enable more flexible and scalable manufacturing of clinically-relevant, high-quality CAR T cells to treat cancers, including solid tumors.

Text

Chimeric antigen receptor (CAR) T cell therapy is rapidly transforming the treatment of many cancers, with five products already approved by the Food and Drug Administration for some hematologic malignancies. However, solid tumors present a difficult challenge for the CAR T field, as clinical trials to date have yielded little to no responses and no improvement in survival[1,2]. Solid tumors have typically been refractory to treatment, due in part to poor T cell potency and persistence within patients[3]. New CAR T products, manufactured for high potency within solid tumors, are critically needed[4–6].

CAR T cells are traditionally manufactured using lentiviruses or γ-retroviruses[7,8] which confer high-efficiency editing; however, viral transduction methods broadly integrate their nucleic acid payloads into the host genome, risking insertional mutagenesis[7,9]. In addition, poorly-specified integration of a CAR transgene can lead to heterogeneous and unpredictable CAR expression. Good manufacturing practice (GMP)-grade viral vectors and associated quality testing are also expensive and constitute a major supply chain bottleneck for the field[10]. Nonviral methods of CAR transduction include transposon-mediated integration[11] and transient mRNA delivery[12]. Like lenti- and retroviruses, transposons also integrate the CAR broadly throughout the genome, while mRNA-mediated delivery results in only transient CAR expression over a period of days. Therefore, standard nonviral delivery methods present vexing challenges for CAR gene transfer.

Recent strategies employing viral vectors and CRISPR/Cas9 editing[13–15] have targeted the CAR transgene to a single genomic locus to reduce the risks of insertional mutagenesis and transgene silencing. Eyquem and colleagues inserted an anti-CD19 CAR into exon 1 of the T cell receptor alpha chain (*TRAC*), disrupting expression of the T cell receptor (TCR) while also driving CAR expression from the endogenous *TRAC* promoter[16]. These AAV-CRISPR-CAR T cells,

engineered through electroporation of Cas9 mRNA followed by delivery of a homology-directed repair (HDR) template within an adeno-associated viral (AAV) vector, were potent, retained a memory phenotype, and showed less exhaustion relative to conventional γ-retroviral products. An AAV-mediated approach has also been combined with TALEN technology to engineer *TRAC*-targeted CAR T cells, with comparable effects on T cell phenotype[17]. These phenotypes correlate with improved outcomes for patients with hematological malignancies[18–25]. Strategies that lead to memory CAR T cell generation with lower exhaustion and terminal differentiation phenotypes have been hypothesized to be beneficial in treating solid tumors[26]. The use of AAVs to deliver the HDR template needed for CRISPR-mediated transgene insertion[16,27] is however severely limited by supply chain challenges associated with viral vector production[10]. Additionally, vector integration into the genome with AAVs can occur when used in conjunction with Cas9[27], and cellular response to introduction of viral elements could affect T cell phenotypes. Therefore, alternate strategies for precise CAR transgene insertion that avoid viral vectors entirely could yield new opportunities to flexibly manufacture CAR T cell immunotherapies.

Nonviral CRISPR/Cas9-mediated gene transfer with transgenic TCR and anti-CD19 CARs have recently been demonstrated to be functional in some cancers, but not for solid tumors[28,29]. Here, we build upon CRISPR-Cas9 genome editing methods[28,30] to integrate a 3 kb third-generation anti-disialoganglioside GD2 CAR transgene at the human *TRAC* locus to report a completely nonviral CAR T cell product featuring the precise genomic integration of a CAR that has been validated in an *in vivo* solid tumor model. HDR within dividing cells has been previously exploited to target transgenes to a single locus using CRISPR-Cas9 genome editing[14,31]. Our manufacturing strategy consistently generates SpCas9-edited, nonviral ("NV")-CAR T cell products at high yields. These NV-CAR T cells demonstrate increased formation of a memory-

like phenotype relative to conventional retroviral ("RV")-CAR T cells at the transcriptional level. These NV-CAR T cells also show evidence of decreased TCR and CAR signaling prior to antigen exposure and comparable potency to conventional viral CAR T cells against GD2+ neuroblastoma *in vivo*.

Results

NV-CAR T cells can be rapidly and reproducibly manufactured with favorable phenotypes. To avoid using HDR donor templates within viral vectors, we first cloned a third generation GD2-targeting CAR sequence[32] into a plasmid containing homology arms flanking the desired cut site at the start of the first exon of the *TRAC* locus (**Fig. 1a**). The same third generation GD2-targeting CAR sequence was used to generate RV-CAR T cells as a comparison throughout this study (**Fig. 1b**). We next generated double-stranded DNA (dsDNA) HDR templates via PCR amplification off the plasmid and performed a two-step purification process to purify and concentrate the templates. In comparison with prior established protocols[28], we performed two sequential purifications on the PCR amplicons to produce a highly-concentrated dsDNA HDR template. Primary human T cells from healthy donors were electroporated with the HDR templates and Cas9 ribonucleoproteins (RNPs) targeting the human *TRAC* locus. Cells recovered for 24 hours at high density in round-bottom multiwell plates and were subsequently expanded in xeno-free media and assayed on days 7 and 9 post-isolation to produce NV-CAR T cell products. As a control, we include an "NV-mCherry" (NV-mCh) condition in which cells harbor the same disruption of the *TRAC* locus, but with a signaling-inert mCherry fluorescent protein inserted in place of the CAR.

We profiled each cell product for viability and yield at various points throughout the manufacturing process. The viability of NV-CAR and RV-CAR T cells were both high (>80%) by

the end of manufacturing (**Extended data Fig. 1a**). Cell proliferation and growth over nine days was also robust for both groups (**Extended data Fig. 1a**). We assessed gene editing at multiple points post-isolation and achieved higher levels of CAR integration when cells were edited at 48 hours after CD3/CD28/CD2 stimulation (**Extended data Fig. 1b**). Using these templates, we achieved consistently high genome editing across over 4 donors. To demonstrate reproducibility of our technique for one donor, we observe ~34% average efficiency of CAR+ and TCR- cells, as measured by flow cytometry (**Fig. 1c-d**). Within the NV-CAR samples, the TCR was knocked out in >90% of T cells (**Fig. 1e**). The mean fluorescence intensity (MFI) of CAR expression was significantly elevated and showed greater range (~1.6 fold; **Fig. 1f**) in the RV-CAR samples in comparison to the NV-CAR samples, indicating decreased CAR expression heterogeneity within the NV-CAR product and consistent with prior findings with AAV-CRISPR-CAR T cells[4].

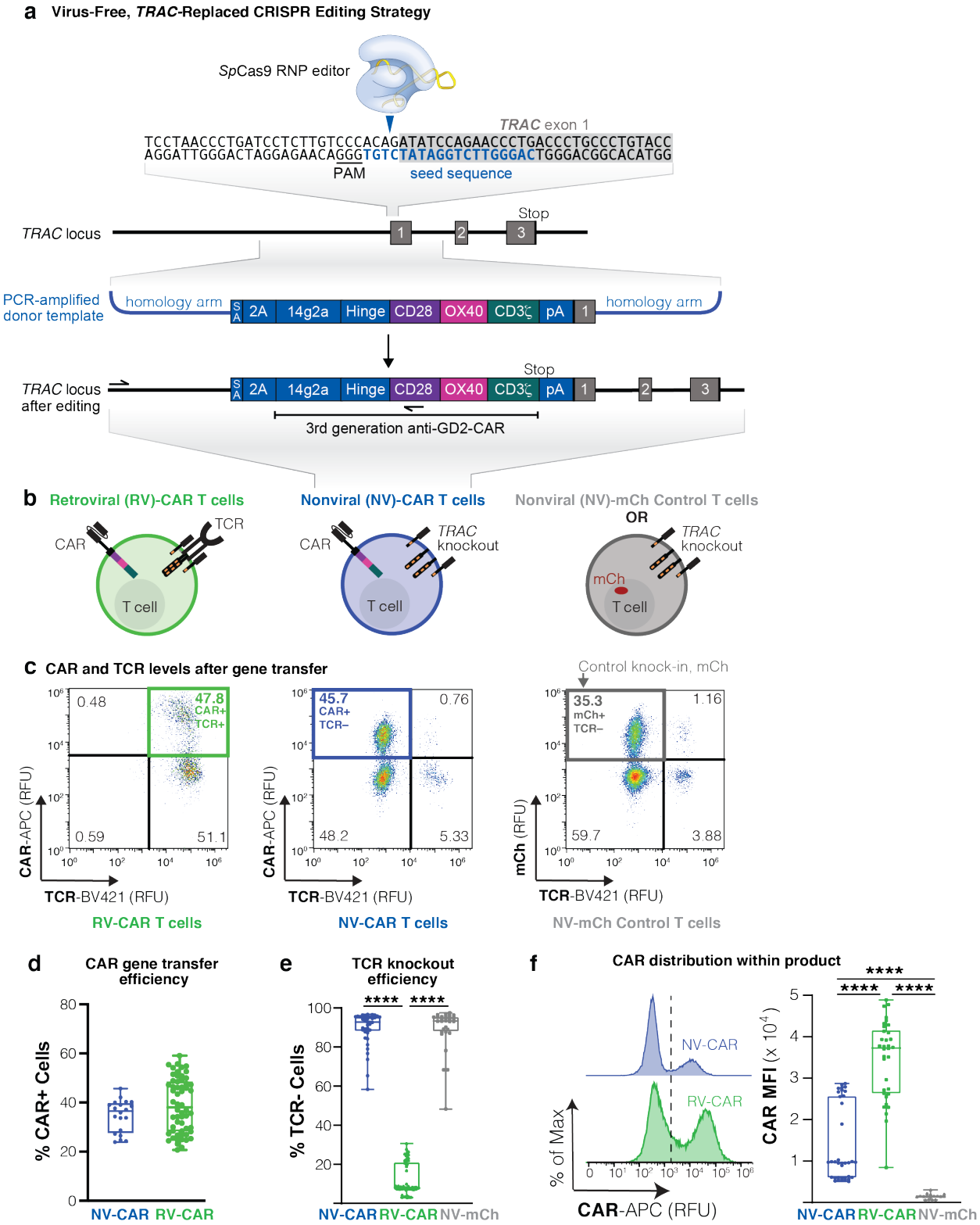

Figure 1. Nonviral (NV) CRISPR-CAR T cells are efficiently generated in one step by replacing the T cell receptor with the CAR. a, Schematic showing the CAR genetic construct and nonviral strategy to insert the CAR into the first exon of the human *TRAC* locus. No viral

components are necessary, and the CRISPR-Cas9 ribonucleoprotein is delivered transiently via nucleofection. The seed sequence of the gRNA is in blue and the protospacer adjacent motif (PAM) for SpCas9 is underlined. 14g2a: single chain variable fragment clone targeting GD2; SA: splice acceptor, 2A: self-cleaving peptide, pA: rabbit ß-globin polyA terminator. Arrows indicate positions of primers for In-Out PCR assay shown in Fig. 2. **b,** Schematic of T cell products used in this study with receptors and expressed transgenes. RV-CAR, donor-matched CAR T cell product generated by retroviral transduction with the same third generation anti-GD2 CAR shown in a; NV-mCh, donor-matched control T cell product manufactured nonvirally as in **a** but with an mCherry fluorescent protein instead of the CAR. **c,** Representative density flow cytometry plots for transgene and TCR surface protein levels on the manufactured cell products. Y-axis shows CAR or mCherry levels and x-axis shows TCR levels on day 7 post isolation (day 5 post-electroporation for NV-CAR and NV-mCh, and day 4 post-transfection for control RV-CAR). Thick black-lined boxes delineate cell populations selected for downstream analysis. Histograms show CAR expression for the three test groups. **d,** Boxplots show the percentage of CAR positive cells from gene editing for NV-CAR cells and from retroviral transduction for RV-CAR cells in each sample. **e,** Boxplots show the percentage of TCR negative cells from gene editing for NV-CAR cells and in RV-CAR cells in each sample. **f,** Mean fluorescence intensity (MFI) values for the CAR expression levels with associated histograms. Boxplots show the percentage of CAR positive cells in each sample. * indicates $p<=0.05$; ** indicates $p<=0.01$; *** indicates $p<=0.001$; **** indicates $p<=0.0001$.

Genomic analysis indicates specific targeting of the CAR transgene to the *TRAC* locus. After confirming robust CAR protein expression, we next performed genomic analysis to measure the on-target specificity of the gene edit. Proper genomic integration of the CAR was confirmed via an "in-out" PCR amplification assay[33] on the genomic DNA extracted from the manufactured cell products with primers specific to the *TRAC* locus and the transgene (**Fig. 2a, Extended Data Fig. 1c**). Next-generation sequencing of genomic DNA to profile any *TRAC* alleles in the cell products without an integrated transgene confirmed high rates of genomic disruption at the *TRAC* locus for these residual alleles, with 93.06% indels for the NV-CAR and NV-mCh samples. Altogether, the combined genomic integration of the CAR or mCherry transgene and indels at the *TRAC* locus resulted in concomitant loss of TCR protein of the T cell surface in sample-matched assays (**Fig 2b, c**). Genome-wide, off-target analysis for our editing strategy was assayed by CHANGE-seq[34]. The top modified genomic site was identified to be the intended on-target site (**Fig. 2d, e**) with a

rapid drop-off for off-target modifications elsewhere in the genome.The CHANGE-seq specificity ratio of our *TRAC* editing strategy is above average (0.056; 57th percentile) when compared to published editing strategies previously profiled by CHANGE-seq[34].

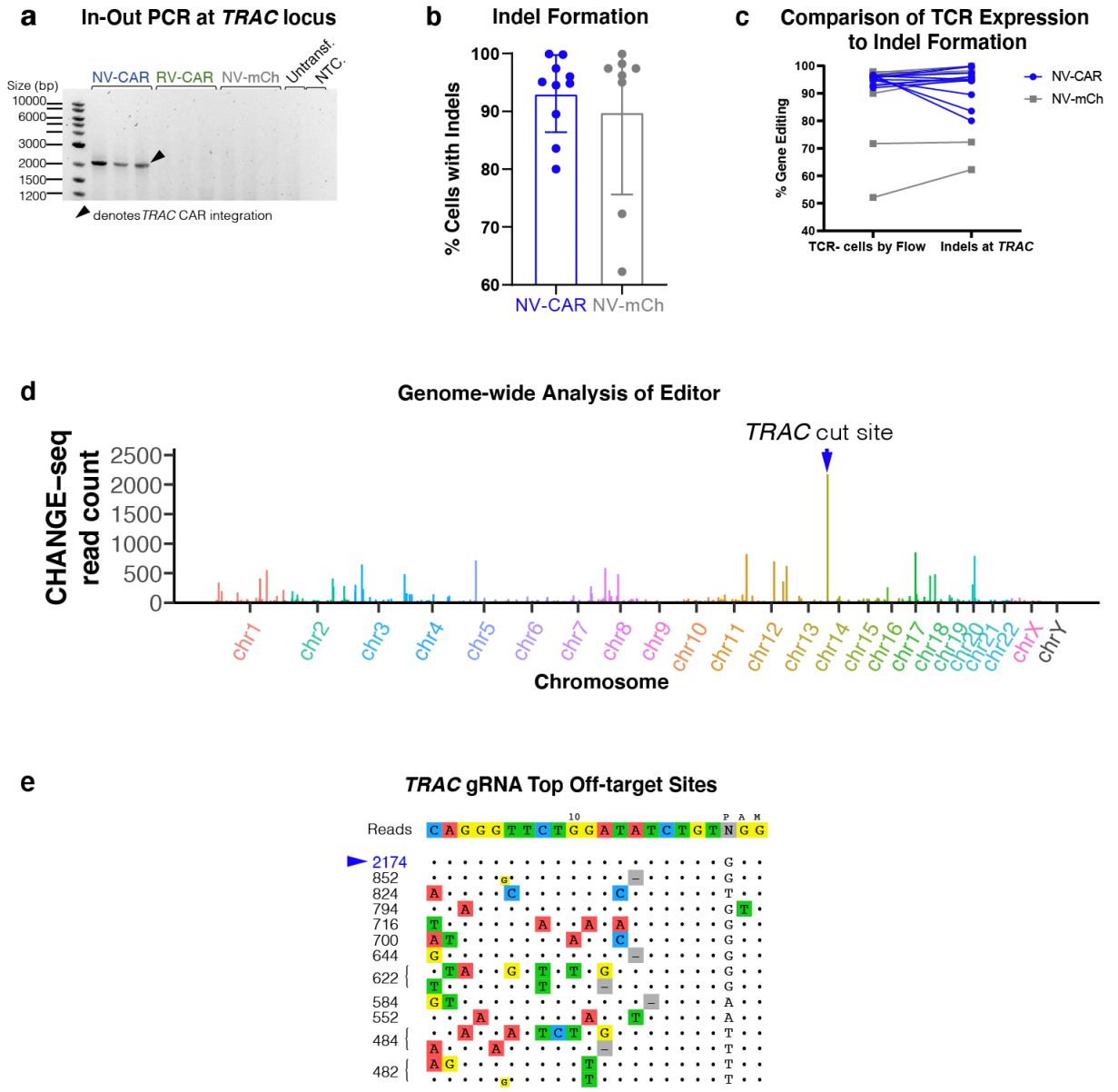

Figure 2. NV-CAR T cells are efficiently and specifically edited at the TRAC locus. a, In-out PCR indicates proper on-target genomic integration of the CAR transgene in NV-CAR cells. Primer locations are shown in Fig. 1a by arrows upstream of the LHA and within the CD28 sequence of the CAR. Untransf., untransfected donor-matched T cells; NTC, non-template control. **b,** Percent of cells with indels at the *TRAC* locus in both NV-CAR and NV-mCh conditions. NV-

CAR (blue) N=10; NV-mCh (grey) N=8, both for one donor. **c,** Level of TCR editing in NV-CAR and NV-mCh T cells measured by both flow cytometry (left) and deep sequencing of genomic DNA (presence of insertions and deletions, indels, at the *TRAC* locus, right). NV-CAR (blue) N=10, NV-mCh (grey) N=8. **d,** Manhattan plot of CHANGE-seq-detected on- and off-target sites organized by chromosomal position with bar heights representing CHANGE-seq read count. The on-target site is indicated with the blue arrow. **e,** Visualization of sites detected by CHANGE-seq. The intended target sequence is shown in the top line. Cleaved sites (on- and off-target) are shown below and are ordered top to bottom by CHANGE-seq read count, with mismatches to the intended target sequence indicated by colored nucleotides. Insertions are shown in smaller lettering between genomic positions, deletions are shown by (-). Output is truncated to top sites.

Cytokine profiling reveals high antigen-specific response for NV-CAR T cells. After harvesting CAR T cells, we profiled secreted cytokines typically associated with a proinflammatory response. On day 9 of manufacturing prior to antigen exposure, RV-CAR T cells produced higher levels of IFNγ, TNFα, IL-2, IL-4, IL-10, IL-13, IL-6, IL-1β and IL-12p70, in comparison to both NV-CAR and NV-mCh T cells (**Fig. 3a**). To test the possibility that RV-CAR T cells produced higher amounts of cytokines regardless of antigen exposure, we performed a 24 hour co-culture between the engineered T cells and GD2+ CHLA20 neuroblastoma, then measured cytokines from the conditioned media. Interestingly, we found that in the presence of antigen stimulation, the previous trend had reversed: NV-CAR T cells either matched or surpassed the level of cytokine production of the RV-CAR T cells (**Fig. 3a**). This result suggests that cytokine production after a single antigen stimulation is comparable in NV-CAR and RV-CAR T cells, regardless of their initial behavior at harvest.

To test the possibility that variation in cytokine production prior to cognate antigen exposure resulted from varying levels of baseline signaling from the CAR and/or TCR during *ex vivo* expansion, we assayed CD3ξ phosphorylation from both native CD3ξ and the CD3ξ portion of the CAR via western blot (**Fig. 3b**). We found elevated protein levels of both CAR and TCR-associated CD3ξ in RV-CAR T cells relative to NV-CAR T cells, potentially indicative of both

high CAR copy number in RV products and an intact TCR-CD3ξ complex in the absence of *TRAC* knockout. We also observed higher levels of CD3ξ phosphorylation in RV-CAR T cells from both CAR and TCR-associated protein, indicating elevated levels of basal signaling. In the absence of antigen exposure, this suggests the presence of tonic signaling, a phenotype that has been associated with an increased propensity for terminal differentiation and exhaustion in some CAR T cell products[35–37]. NV-CAR and NV-mCherry cells both showed sharply decreased TCR-mediated CD3ξ signaling after *TRAC* knockout, and NV-CAR T cells also showed very little activity from CAR-associated CD3ξ. This is consistent with prior findings that TCR replacement with a CD19 CAR can decrease CAR-mediated tonic signaling by driving expression by the native *TRAC* promoter[16].

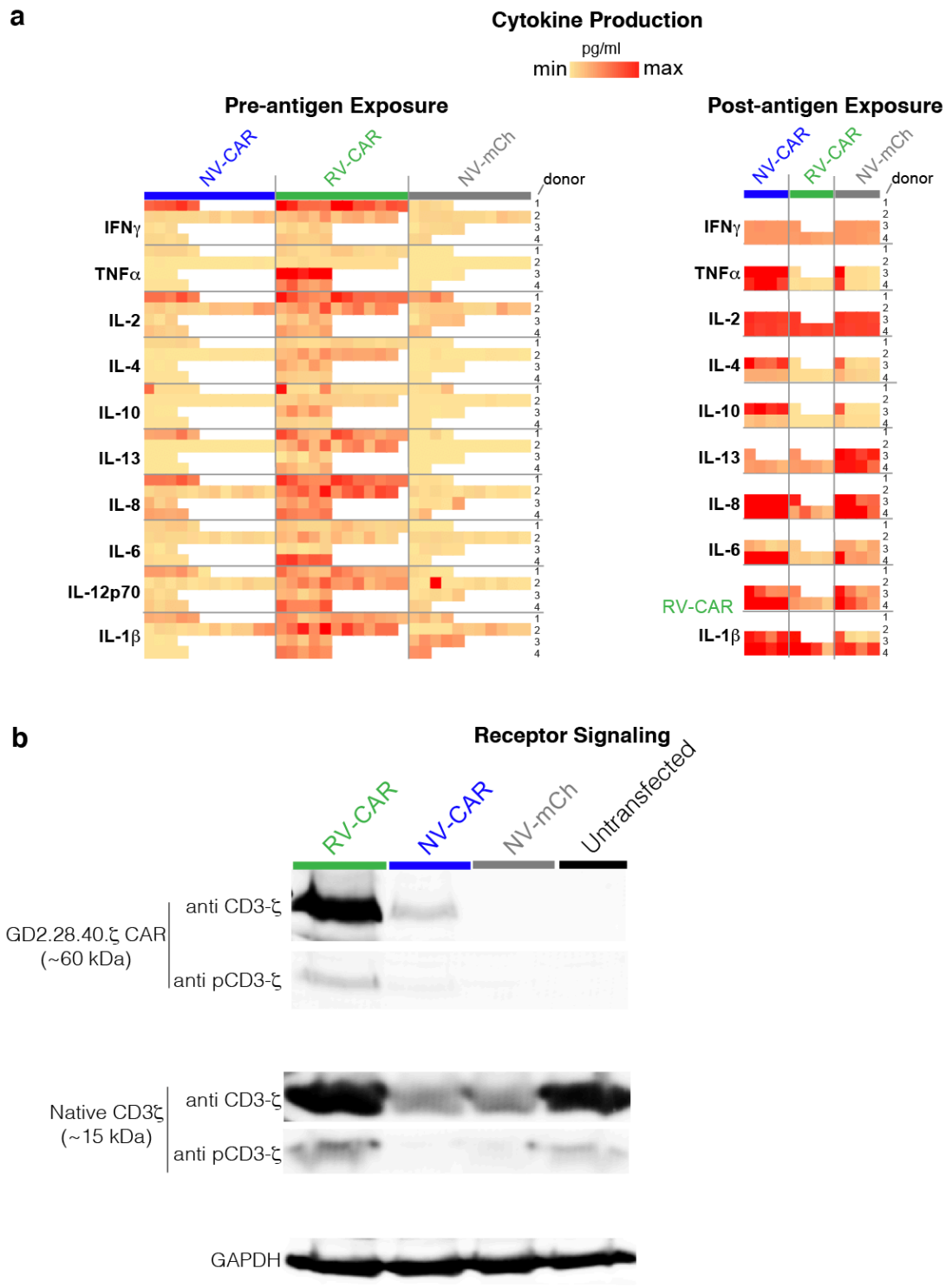

Figure 3. NV-CAR T cells mount robust cytokine response upon exposure to cognate antigen, and decreased CAR and TCR-mediated tonic signaling. a (left), Cytokine production from conditioned media taken from T cell products at the end of manufacturing (pre-antigen exposure).

Values are pooled from all four donors. NV-CAR (blue) N=24; RV-CAR (green) N=33; NV-mCherry (gray) N=22. **a (right),** Cytokine production in conditioned media after a 24 hour co-culture of manufactured T cell products with the target GD2-antigen on CHLA20 neuroblastoma cells. Values are pooled from two donors. NV-CAR (blue) N=8; RV-CAR (green) N=5; NV-mCh (gray) N=8. The minimum and maximum for the color scale for each cytokine is as follows: IFN-y, 2000-30000 pg/mL. TNF-a, 10-1000 pg/mL. IL-2, 700-6000 pg/mL. IL-4, 0.2-20 pg/mL. IL-10, 0.5-150 pg/mL. IL-13, 300-1100 pg/mL. IL-8, 25-1800 pg/mL. IL-6, 10-400 pg/mL. IL-p70, 0.1-4 pg/mL. IL-1b, 0.2-100 pg/mL. **b,** Western blot from cell lysates featuring 40% transgene+ cells and stained for CD3z, pCD3z, and GAPDH. Native CD3z and GD2.28.40.z. CD3z domains were distinguished by molecular weight (15 and 60 kDa, respectively). N=1 donor.

Transcriptional signatures prior to target antigen exposure reveals aberrant signaling in RV-CAR T cells. To further define the phenotypic differences between NV-CAR, NV-mCh, and RV-CAR T cells, we performed single-cell RNA-sequencing (scRNA-seq) on 79,317 cells from two different donors, both at the end of the manufacturing process and after 24 hours of co-culture with GD2+ CHLA20 neuroblastoma cells (**Fig. 4a**). We observed no significant donor-specific or batch effects, as indicated by gross clustering patterns in the combined data set. Further, we observed no significant changes in transcript levels for genes at or within 5 kb of off-target sites predicted by CHANGE-seq, indicating that any potential genomic disruptions at these sites did not lead to detectable changes in proximal transcripts. To distinguish edited transgene-positive and transgene-negative cells within each sample, we aligned reads to a custom reference genome containing an added sequence mapping to the CAR or mCherry transgenes. Subsequent transcriptional analyses were carried out on transgene-positive cells only within each sample (21,068 cells total).

We performed tSNE dimensionality reduction and clustering on all cells and identified clusters with gene expression patterns associated with various phenotypes, including memory-like and effector-like populations across CD4 and CD8 subsets (**Fig. 4a**). We examined the distribution of transgene+ cells within each cluster, and found that prior to antigen stimulation,

55% of NV-CAR and 61% of NV-mCherry T cells fell into clusters with a memory-like phenotype, while only 25% of RV-CAR T cells did so; conversely, 49% of RV-CAR T cells at harvest had effector-like phenotypes, while 33% of NV-CAR T cells and 27% of NV-mCherry T cells fell into these clusters (**Fig. 4b**). This suggests that prior to cognate antigen exposure, *TRAC* knockout plays a role in memory formation and maintenance of a less differentiated phenotype, as measured at the transcriptional level. This finding was corroborated by elevated CD62L protein expression in both NV-CAR and NV-mCh cells relative to RV-CAR cells, as measured by flow cytometry (Fig 4c). The mean fluorescence intensity (MFI) of CD62L increased by approximately three-fold in the NV-CAR T cells relative to the RV-CAR T cells. Increased CD62L is consistent with TRAC-CAR T cells featuring a CD19 CAR[16], and may indicate elevated memory formation after manufacturing, although additional protein-level data are needed to confirm this hypothesis (**Fig. 4c**).

Notably, we observed that the skew toward a memory-like phenotype at the transcriptional level did not persist for NV-CAR or RV-CAR T cells after cognate antigen exposure. After 24 hours of co-culture with GD2+ neuroblastoma cells *in vitro*, the distribution of transgene+ cells within each cluster shifted such that 27% of NV-CAR and 21% of RV-CAR T cells expressed memory-associated transcriptional signatures, while 60% of NV-mCherry cells expressed this phenotype; conversely, 53% and 59% of NV-CAR and RV-CAR T cells expressed effector-like transcriptional signatures after coculture, while only 24% of NV-mCherry cells did so. This indicates that both NV and RV CAR T cells can mount a robust effector response, while NV-mCherry cells lacking either a CAR or TCR retain their less-differentiated phenotype when exposed to cancer.

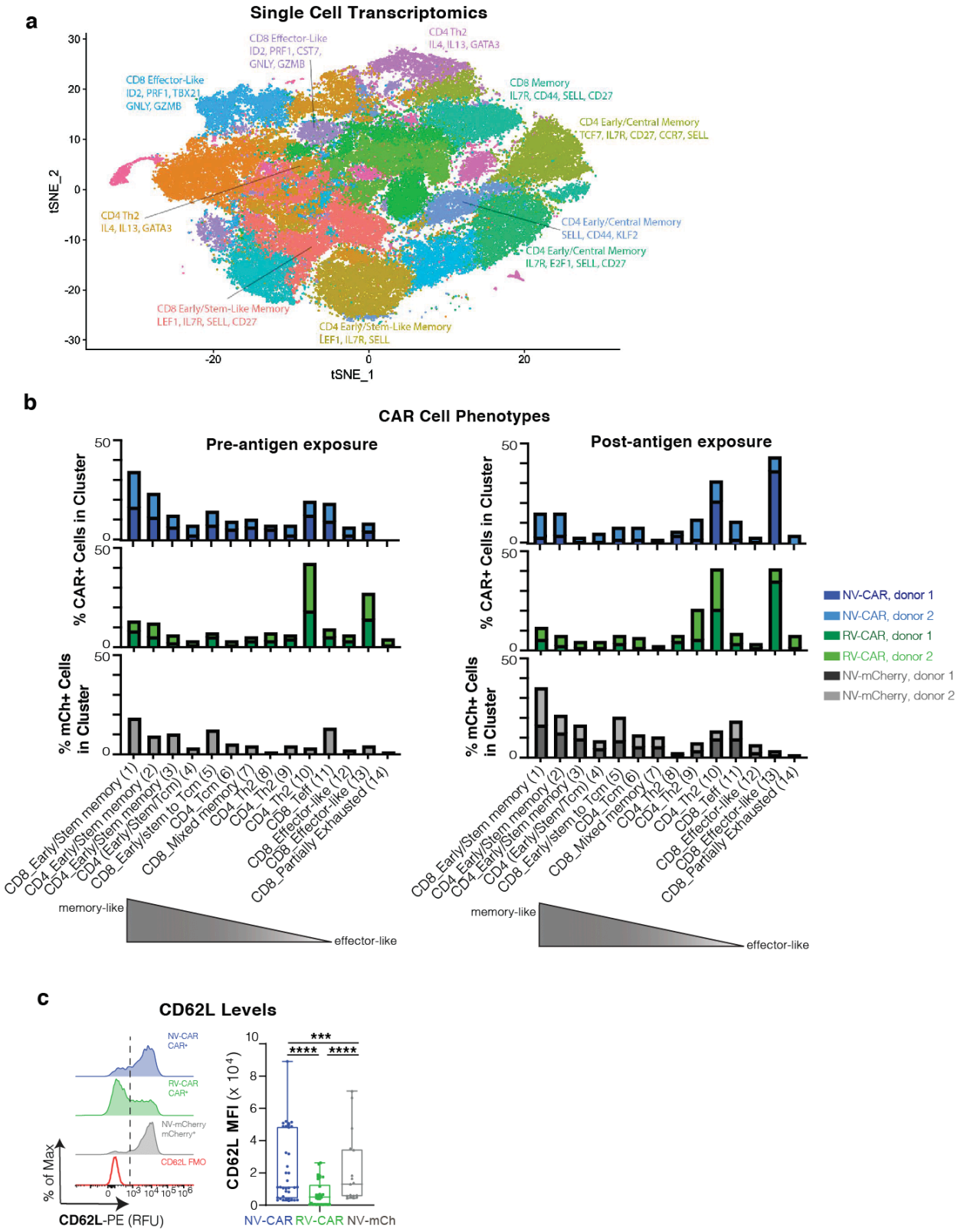

Figure 4. Transcriptional signatures prior to target antigen exposure reveals elevated memory formation in *TRAC*-knockout products, . a, tSNE projection of single cell RNA-seq

data from 15 samples of manufactured cell products, both pre- and post-antigen exposure; 79,317 single cells from NV-CAR, RV-CAR, NV-mCh and untransfected T cell products are shown. **b,** Proportion of transgene+ cells (21,068 total cells) within each annotated cluster. **c**, Histograms show CD62L expression for the three test groups. Boxplots show mean fluorescence intensity (MFI) for CD62L expression. NV-CAR (blue) N=31; RV-CAR (green) N=39; NV-mCh (gray) N=27. Replicates from 97 total samples across 4 separate donors.

NV-CAR T cells demonstrate potent *in vitro* killing of GD2-positive cancer cells. After characterizing cellular phenotypes and gene expression at the end of the manufacturing process, we measured the *in vitro* potency of NV-CAR T cells against two GD2-positive solid tumors: CHLA20 neuroblastoma and M21 melanoma (**Fig. 5a**). We performed both a fluorescence-based cytotoxicity assay, measuring loss of expression from fluorescently labeled cancer cells over time (**Fig 5b**), and IncuCyte live cell analysis at 2-hour intervals over a 48 hour period (**Fig. 5c**). We observed potent killing using a 5:1 effector:target ratio for both NV-CAR and RV-CAR T cells, using both assays. These results corroborate our finding that NV-CAR T cells produce proinflammatory cytokines and upregulate a cytotoxicity-associated gene signature at levels comparable to RV-CAR T cells, and demonstrate potent target cell killing for multiple GD2+ cancers of variable origin.

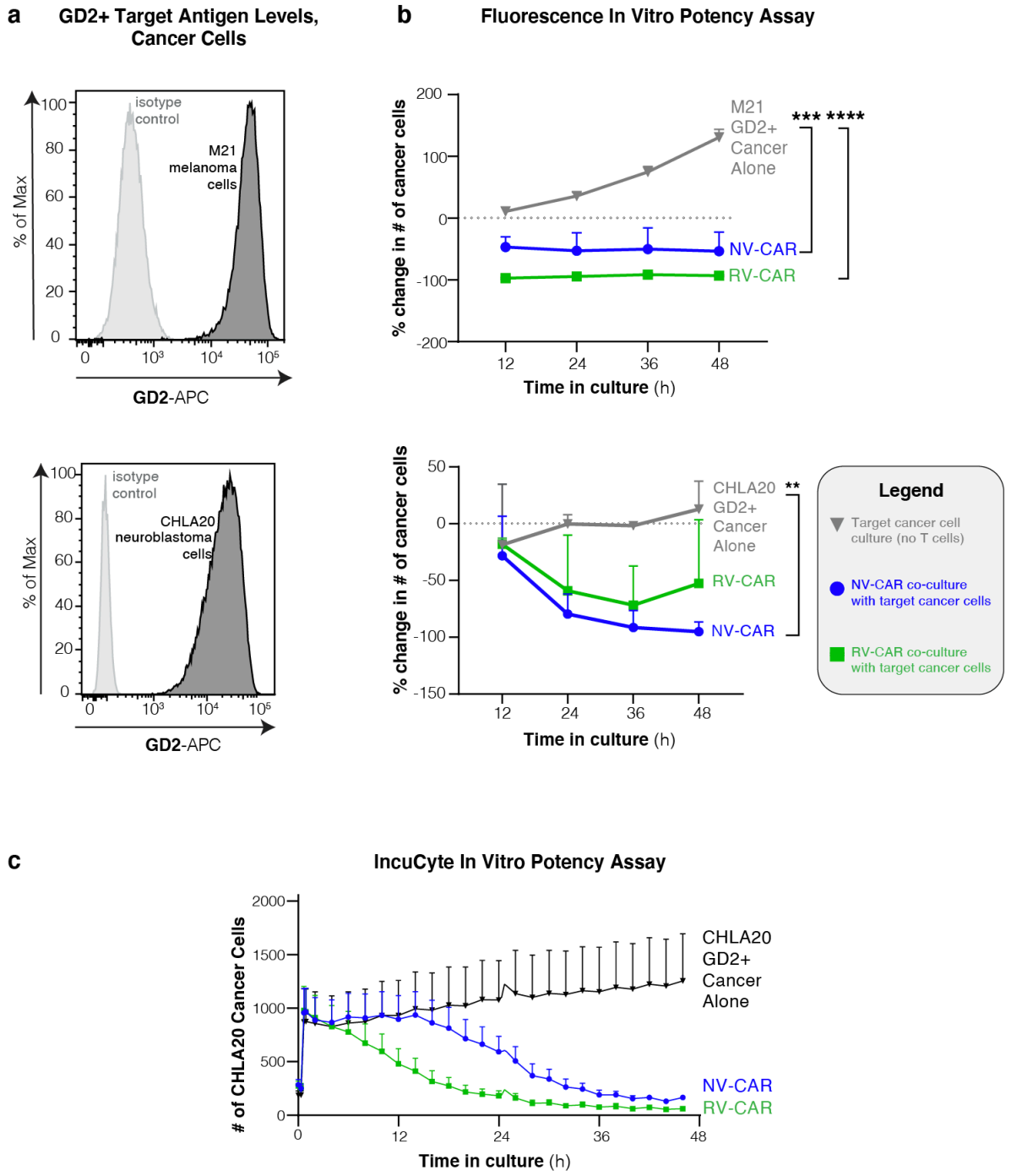

Figure 5. NV-CAR T cells demonstrate robust *in vitro* killing of GD2+ cancer cells. a, Flow cytometry histograms show GD2 surface expression on M21 and CHLA20 cell lines (black) compared to isotype controls (gray). **b,** Graphs show the cytotoxic action of NV-CAR and RV-CAR T cells against two GD2-positive tumor cell lines, CHLA20 and M21, containing a stably integrated fluorescent transgene (AkaLuc-GFP and H2B-mCherry, respectively). Cytotoxicity was measured by change number of mCherry-positive objects for each image. The assay was

performed using cells manufactured from one donor. **c,** IncuCyte *in vitro* assay of T cell potency, averaged across four donors. AnnexinV was added as a marker of cell death; y-axis shows GFP-positive cancer cells in each well of a 96-well plate. The ratio of T cells to cancer cells is 5:1. The consistent decrease in CHLA20 cells after 15 hours indicates high potency of both NV-CAR and RV-CAR T cells. NV-CAR (blue) N=12; RV-CAR (green) N=12; CHLA20 neuroblastoma alone (black) N=9. *indicates p<=0.05; ** indicates p<=0.01; *** indicates p<=0.001; **** indicates p<=0.0001.

NV-CAR T cells demonstrate robust *in vivo* regression of GD2-positive neuroblastoma. Because important clinical cell behaviors like homing, persistence and cytotoxicity within a tumor microenvironment cannot be easily assessed *in vitro*, we assessed CAR T cell potency *in vivo* in an established human GD2+ neuroblastoma xenograft model. After 9 total days of culture, multiple replicate wells of RV-CAR, NV-CAR, or NV-mCh T cells were pooled for injection into NOD-SCID-$\gamma c^{-/-}$ (NSG) mice (Jackson Laboratory). Ten million T cells were delivered via tail vein injection to each NSG mouse with an established luciferase-expressing CHLA20 neuroblastoma solid tumor identified by bioluminescence (**Fig. 6a**). Tumor sizes were quantified over time by IVIS imaging and digital caliper. Both CAR-treated cohorts showed robust tumor regression in the first 3 weeks post-infusion (**Fig. 6b, Extended Data Fig. 2a, b**). These cohorts also showed significantly improved survival relative to NV-mCh-treated mice; however, there was no significant difference in survival between NV-CAR and RV-CAR treated mice by day 80 (p-value=0.4099, n.s.; **Fig. 6c**). The percentage of CAR-positive cells per dose was lower in NV-CAR T cells versus RV-CAR T cells (17.8% vs. 39.9%), which may have contributed to a slight decrease in complete remission rates (5/8 RV-CAR vs. 4/9 NV-CAR). Inconsistencies in initial tumor burden likely also affected remission. None of the control NV-mCh mice showed tumor regression, and all seven mice died of tumor progression by day 60, implying that disease control was antigen specific. We also assessed persistence, memory and exhaustion phenotypes in CAR T

cells isolated from the spleens and tumors of CHLA20-bearing mice. NV-CAR T cells persisted in both the spleens and tumors of the treated mice, but not for NV-mCh T cell treatments, indicating successful trafficking of NV-CAR T cells to the tumor (**Fig. 6d-f, Extended Data Fig. 2c**). Additionally, we observed that cells in the spleen had lower levels of PD-1, LAG-3 and TIM-3 exhaustion markers after NV-CAR treatment relative to the RV-CAR treatment in lymphocytes recovered from the spleen (**Fig. 6e-g, Extended Data Fig. 2d).**

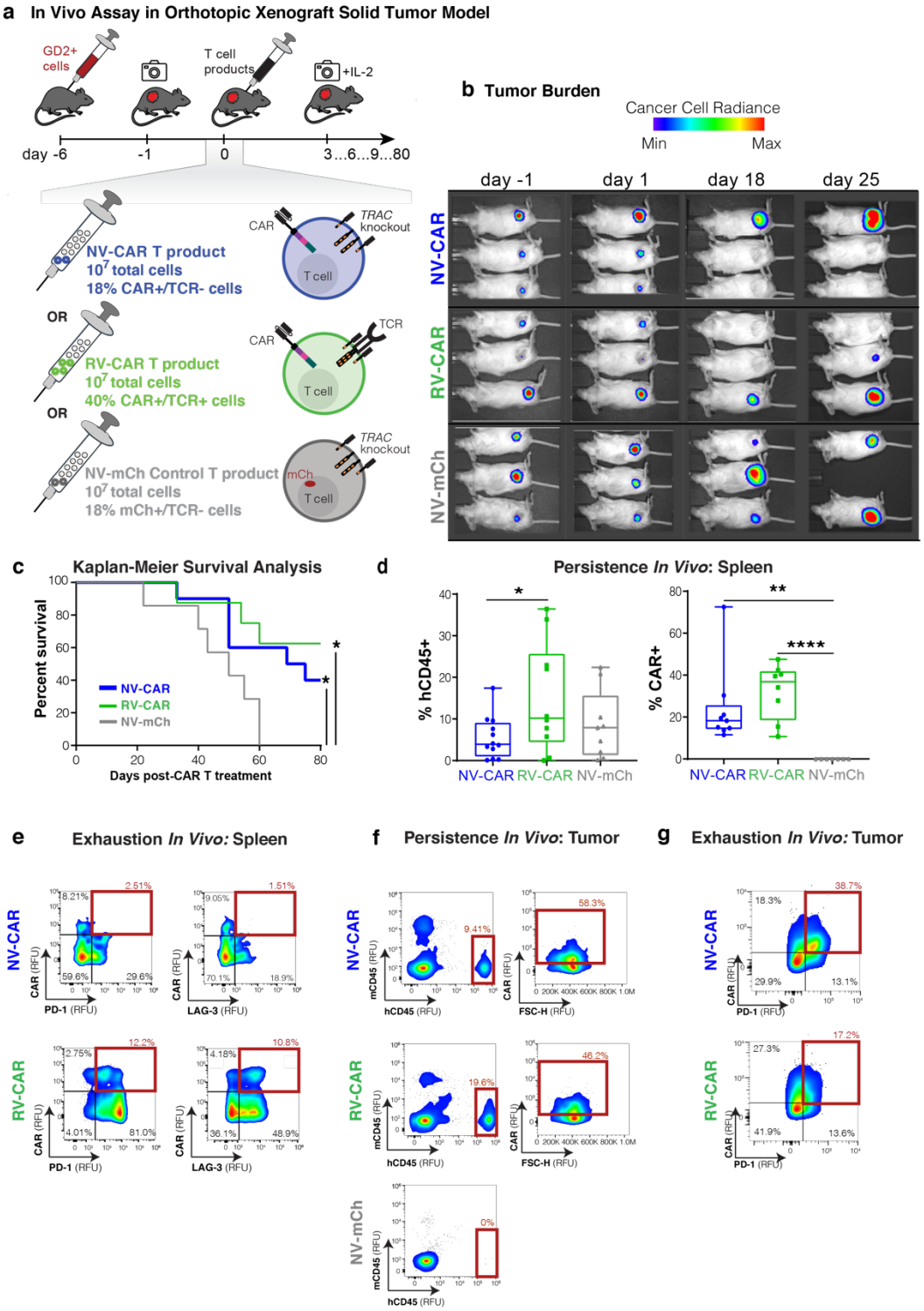

Figure 6. NV-CAR T cells induce robust regression of GD2+ neuroblastoma solid tumors *in vivo*. a, Schematic of the *in vivo* mouse dosing strategy using NSG mice harboring GD2-positive CHLA20 neuroblastoma tumors. **b,** Representative IVIS images of NSG mice with CHLA20 tumors that were treated with either 10 million NV-CAR, RV-CAR, or NV-mCh T cells. **c,** Kaplan-Meyer survival curve for mice. NV-CAR (blue) N=10; RV-CAR (green) N=8; NV-mCh (gray)

N=7. **d,** Box plots show presence of CAR+CD45+ human T cells in mouse spleens, as measured by flow cytometry. **e,** Flow cytometry plots showing levels of PD-1 and LAG-3 on the human lymphocytes (CD45+) cells collected from mouse spleens. **f**, Flow cytometry plots show human CD45+CAR+ NV-CAR and RV-CAR T cells are found in tumors, but NV-mCh cells are not. **g**, Flow cytometry plots showing levels of PD-1 on human CD45+ lymphocytes collected from mouse tumors.

Finally, we matched the absolute number of CAR positive cells infused between nonviral and retroviral products in a separate animal study (**Fig. 7**). NSG mice harboring human GD2+ xenograft tumors were infused with 10 million cells from three different T cell products. The percentage of CAR positive cells were approximately the same, 40%, in both the NV-CAR and RV-CAR products. The NV-Control product also had 38% transgene positive cells. After a month, all four mice treated with RV-CART cells had higher adverse clinical scores indicative of xeno-graft-vs-host-disease (xeno-GvHD; **Fig. 7b-c**). The lack of xeno-GvHD in the mice treated with NV-CART and NV-Control products indicates a functional knockout of TCR signaling by our CRISPR-Cas9 editing strategy. In contrast, three of the four mice treated with NV-CART products were event-free and survived past 96 days (**Fig. 7d-e**). Again, we assessed persistence, memory and exhaustion phenotypes in human lymphocytes recovered from the spleen and tumors of CHLA20-bearing mice. CAR T cells persisted in the spleens for all products (24%, 36±19%, and 23±7.6% human CD95+ cells within the spleen for NV-CAR, RV-CAR and NV-mCh, respectively). Additionally, we observed that nonviral human cells in the spleen had higher levels of CD62L memory markers relative to the RV-CAR treatment**.** For the non-responding mice, NV-CAR and RV-CAR T cells were robustly detected in tumors upon euthanasia of the treated mice, but almost no NV-mCh T cells could be detected in their tumor counterparts (12%, 29%, and 0.058±0.046% human CD95+ cells within the tumor for NV-CAR, RV-CAR and NV-mCh, respectively). These data indicate successful trafficking of NV-CAR T cells to the tumor.

Altogether, these findings demonstrate comparable potency of NV-CAR T cells to standard RV-CAR T cells, establishing the potential clinical relevance of NV-CAR T cells for treating solid tumors.

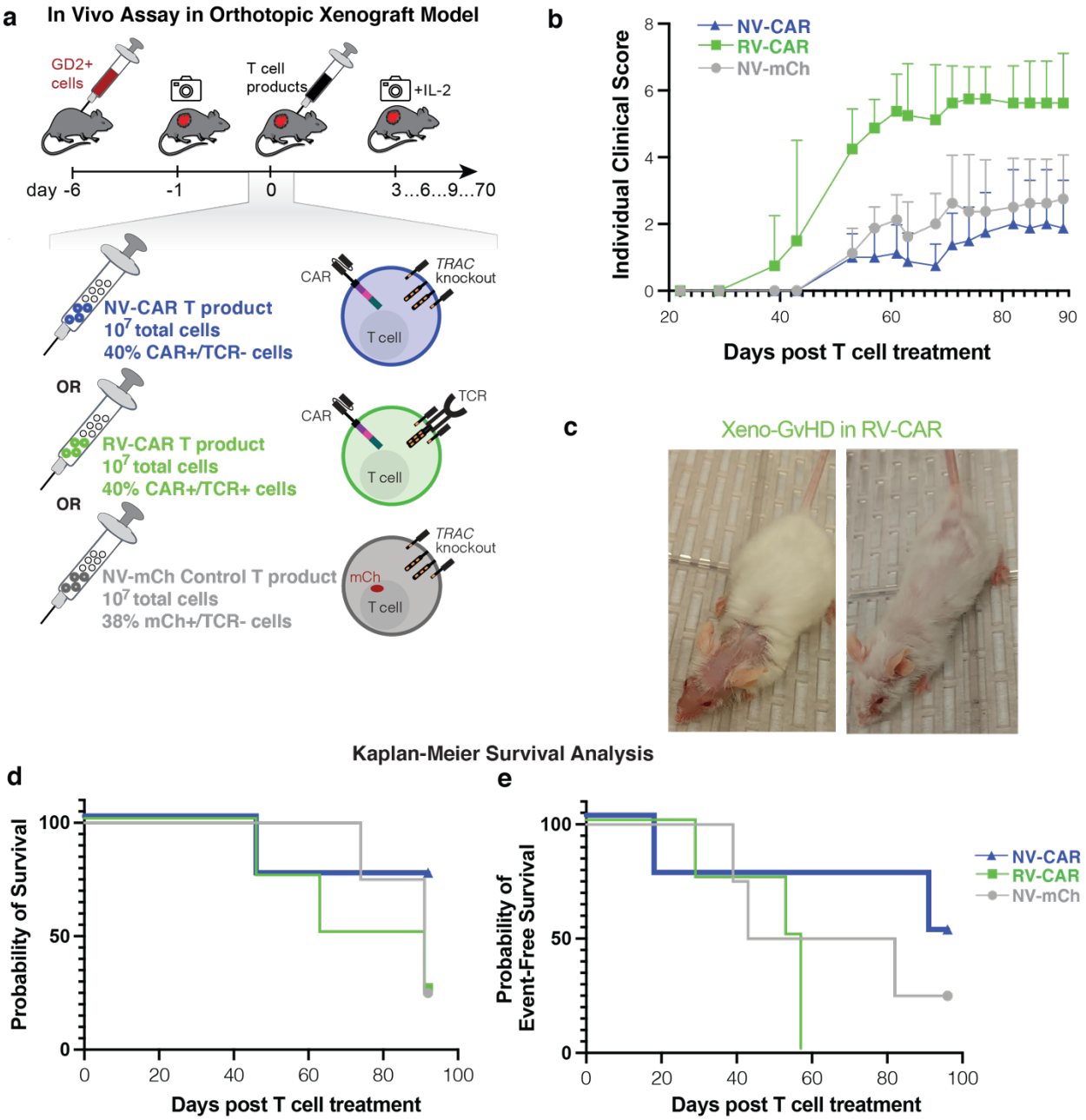

Figure 7. Nonviral CART cells exhibit *in vivo* potency against GD2+ solid tumors with high event-free survival. (**a**) Timeline of T cell product infusion into orthotopic CHLA20 GD2+ solid tumors. GD2+ solid tumors were established in the side flank of each mouse as detected by IVIS imaging at day -1. At day 0, three different CART products as shown below were infused

into the tail vein. (**b**) Adverse clinical score of each mouse treated. Higher score indicates more adverse symptoms observed in the mice. (**c**) Pictures of RV-CAR T-treated mice showing xeno-GvHD symptoms from the intact TCR function within the RV-CAR T cells. None of the mice infused with nonviral TRAC-edited products displayed signs of xeno-GvHD. (**d-e**) Kaplan-Meier overall survival (**d**) and event-free survival (**e**) of mice treated with the three different T cell products. An event was defined as the appearance of a palpable tumor or a clinical score of 4 or above. NV-CART treated mice had the highest probability of event-free survival.

Discussion

Historically, CAR T cells have exhibited frustratingly limited success against solid tumors. While anti-GD2 CAR T cells were the first to mediate regression of a solid tumor[38] in patients, the effects ultimately were not durable due in part to poor T cell persistence[26]. The third generation CAR used in this study failed to mediate meaningful anti-tumor responses in patients when delivered as a retroviral construct[39]; therefore, we sought to determine whether a TRAC-CAR replacement strategy, previously shown to be successful in the context of a CD19 CAR, could improve outcomes. Extensive work has focused on overcoming the immunosuppressive tumor microenvironment; however, there is an urgent need for new engineering strategies to make the cell product itself more potent, whether through armored CARs, T cell selection procedures, combinatorial therapies. or other approaches[40–42]. Leveraging prior work on hematological malignancies where anti-CD19 AAV-CAR T cells were manufactured using AAV and SpCas9[16], we develop a completely nonviral workflow that can accommodate a large CAR template (~3kb) targeting a solid tumor antigen, GD2. Our findings open new avenues for manufacturing high-quality and defined genome-edited, NV-CAR T cells to treat solid tumors.

Here we describe reproducible, nine-day manufacturing of third generation GD2-specific CAR T cells using recombinant SpCas9 protein and nucleic acids. Our manufacturing process produced similar yields across four donors and resulted in stable, genomically-integrated, durable CAR expression (>80 days *in vivo*) without the use of any viral vectors or animal-

derived components during gene transfer or scale up. The decrease in T cell viability linked to nucleofection[43] is transient in our workflow with cells recovering to >80% viability just one week after nucleofection, satisfying typical regulatory thresholds. Our use of high-density culture to improve T cell aggregation may stimulate pro-survival cell-cell signaling to overcome stress arising from nucleofection. Furthermore, cell proliferation is likely to have an added benefit, as homologous recombination is active in the S and G2 phases of the cell cycle and increases in HDR have been observed in cycling cells[44]. We also improve the ease of manufacturing the HDR repair template by performing two sequential Solid Phase Reversible Immobilization-based purification steps on the PCR products. This purification procedure concentrates the template and is facile, keeping preparation time and cost-per-reaction low. Further, we do not rely on excipients to increase editing efficiency, which have been proposed recently[45], and thereby provide a streamlined gene transfer process. Altogether, these methodological changes constitute an important advance for the adoptive T cell therapy in enabling clinically relevant, rapid, and efficient nonviral CAR T cell manufacturing.

In retroviral CAR T products, vector copy numbers can vary,[46,47] and genomic integration is scattered across >10,000 sites in the human genome[3]. The CAR expression in retroviral products therefore can be affected by both the copy number and various chromatin contexts of each vector integrant across the various cells in a product. In contrast, our strategy inserts the CAR at a single site (*TRAC*) at a copy number of 1 or 2, where the CAR transgene is driven by only one promoter, the endogenous *TRAC* promoter. CRISPR strategies with AAV donor templates integrate, at 5-20% frequencies, the entire AAV vector into the Cas9-induced DNA double strand break[48] and therefore may disrupt *TRAC* regulation. Hence, variable CAR expression within a cell product can depend on the degree of AAV vector integration. Thus, usage of a virus-free CRISPR strategy can

reduce variability in CAR expression (**Fig. 1f**). Undesired genomic alterations and adverse events arising from genome editing are low: the on-target specificity of our editor is above average when compared to many other editing strategies[34], with no detectable transcriptional changes in genes at or proximal to predicted off-target sites in the edited cells. Our strategy to use SpCas9 as RNPs versus encoded on mRNAs[16,49–51] reduces the lifetime of active SpCas9 proteins within the cell (hours for RNP versus days for mRNA). This highly-transient induction of DNA double strand breaks by SpCas9 RNPs in our strategy likely contributes to the high specificity of genomic modifications to the *TRAC* on-target site, as increased off-target effects have been previously seen with prolonged presence of SpCas9 within cells[52].

There is a paucity of knowledge regarding the signaling effects of CAR expression in T cell products. We show evidence of decreased receptor signaling in the NV-CAR T cell product at the level of the secretome and CD3z phosphorylation. Our results indicate that, in addition to altering the design of the CAR itself, the locus of insertion and the absence of TCR expression can affect receptor signaling. Reduced CAR and TCR tonic signaling during manufacturing could be notably important for allogeneic workflows involving stem cell sources (e.g., induced pluripotent stem cells[53–55], hematopoietic stem cells[56], umbilical cord blood[57], etc.), where developmental signaling for proper specification towards effector cell types may be disrupted by receptor signaling during differentiation. Our large-scale scRNA-seq dataset profiling CAR T cells with varied receptor signaling profiles, both with and without antigen exposure and across multiple donors in this study, could be a useful resource for analyzing the effects of CAR transgenes within human immune cell products.

The phenotype of the NV-CAR T cell product could be advantageous for future clinical purposes. Cytokine production is lower in NV-CAR T cells prior to antigen exposure, but

equivalent to or higher than RV-CAR T cells post-antigen exposure, suggesting a higher dynamic range of antigen-driven potency. The NV-CAR T cells also demonstrate increased expression of the memory-associated receptor CD62L relative to RV-CAR T cells. This quality attribute is directly correlated with improved rates of durable remission with CD19 CAR T cells for hematologic malignancies[18,58]. Prior work with hematopoietic stem/progenitor cells indicated that the AAV template itself elicited both immune and stress responses, along with transcriptional downregulation of cell cycle processes that could interfere with stem cell maintenance[59]. Switchable anti-CD19 CARs have demonstrated increased CD62L+ memory formation upon turning off CAR signaling, indicating that prolonged or tonic CAR signaling can interfere with memory formation[60]. These studies reference and are consistent with prior work where overstimulation of TCR signaling and CD28 co-stimulatory signaling can affect unmodified T cell differentiation *in vivo*, as memory responses in vivo with unmodified T cells are formed through acute, high-load antigen stimulation followed by a "rest" phase[61]. Future studies may also reveal additional mechanistic connections between these observations.

After injection into a GD2-positive human neuroblastoma xenograft model, NV-CAR T cells induce strong regression of solid tumors compared to mock-edited T cells, and at levels comparable to RV-CAR T cells. In our first *in vivo* experiment, comparable tumor regression rates occurred in spite of the substantially lower proportion of CAR+ cells in the NV-CAR product. In our second *in vivo* experiment, we observed that cell-for-cell, an NV-CAR T cell product could lead to a potent *in vivo* response with longer event-free survival. The TCR knockout by our editing strategy is functionally validated in this second study as xeno-GvHD was significantly delayed or eliminated altogether for the mice treated NV-CAR and NV-Control products.

Finally, nonviral genome editing workflows confer critical advantages in scale-up/out and biomanufacturing. Relative to conventional T cell manufacturing, our streamlined, nonviral manufacturing process could: *1)* reduce the batch-to-batch variability, supply chain challenges, and costs associated with vector production[8,62], *2)* alleviate a number of regulatory considerations related to the need for monitoring replication competency of the vector and the levels of xenogeneic components in the clinical cell product, notably plasmid DNA and serum during the gene transfer and scale up process that can introduce infectious agents or toxic components[63]; and *3)* eliminate the potential for integration of viral elements into the human genome, which can generate a high degree of gene perturbation, up to 10^4-10^5 different insertional sites within a single product[9]. Integration of the vector, in particular, presents risks of insertional oncogenesis[64], transgene silencing or overexpression, and adverse immune response to the vector, which could result in the rejection of therapeutic cells. While off-target analysis of genome editors is necessary for any clinical translation of our approach, there are now many experimental and computational tools that can readily be used for this purpose[34,65] and next-generation high-fidelity Cas9 enzymes[66] could be used to further decrease the potential for any off-target effects. Overall, a nonviral editing workflow has high potential to enable the rapid and flexible manufacture of highly defined and highly potent CAR T cell products for the treatment of solid tumors.

Methods

Cell lines. CHLA20 human neuroblastoma cells were a gift from Dr. Mario Otto and M21 human melanoma cells were a gift from Dr. Paul Sondel (University of Wisconsin-Madison). These cells were maintained in Dulbecco's Modified Eagle Medium high glucose (Gibco) supplemented with

10% Fetal Bovine Serum (Gibco) and 1% Penicillin-Streptomycin (Gibco). AkaLUC-GFP CHLA20 cells were a gift from Dr. James Thomson (Morgridge Institute for Research). Phoenix cells (ATCC) for viral preparation were maintained in DMEM (high glucose) supplemented with 10% Fetal Bovine Serum (Gibco) and selected using 1 µg/mL diphtheria toxin (Cayman Biologics) and 300 µg/mL hygromycin (Thermo Fisher Scientific) prior to use. Selection for transgene positive cells was confirmed by flow cytometry for mouse Lyt2 expression (Biolegend) (>70%+). 3T3 cells were maintained in Dulbecco's Modified Eagle Medium (Gibco) supplemented with 10% Fetal Bovine Serum (Gibco) and 1% Penicillin-Streptomycin (Gibco). Cell authentication was performed using short tandem repeat analysis (Idexx BioAnalytics, Westbrook, ME) and per ATCC guidelines using morphology, growth curves, and *Mycoplasma* testing within 6 months of use with the e-Myco mycoplasma PCR detection kit (iNtRON Biotechnology Inc, Boca Raton, FL). Cell lines were maintained in culture at 37°C in 5% CO_2 and used after 3-5 passages in culture after thawing.

Plasmid constructs. NV-*TRAC*-CAR: A 2kb region surrounding the *TRAC* locus was amplified by PCR from human genomic DNA and cloned into a pCR blunt II TOPO backbone (Thermo Fisher Scientific). The CAR transgene from a pSFG.iCasp9.2A.14G2A-CD28-OX40-CD3z RV-CAR plasmid (gift from Dr. Malcolm Brenner, Baylor College of Medicine) was then cloned into the TOPO *TRAC* vector using Gibson Assembly (New England Biolabs (NEB)). The plasmid sequence was verified by Sanger sequencing. The NV-TRAC-mCherry construct was designed in house, synthesized, and sequence-verified (GenScript). All plasmids were grown in 5-alpha competent *E. coli* (NEB) and purified using the PureYield MidiPrep system (Promega).

Double-stranded DNA HDR template production. Plasmid donors were used as PCR templates for NV products. In brief, NV-CAR and NV-mCh plasmids were MidiPrepped using the PureYield MidiPrep system (Promega). PCR amplicons were generated from plasmid templates using Q5 Hot Start Polymerase (NEB) and pooled into 100 µl reactions for Solid Phase Reversible Immobilization (SPRI) cleanup (1X) using AMPure XP beads according to the manufacturer's instructions (Beckman Coulter). Each 100 µl starting product was eluted into 5 µl of water. Bead incubation and separation times were increased to 5 minutes, and elution time was increased to 15 minutes at 37°C to improve yield. PCR products from round 1 cleanup were pooled and subjected to a second round of SPRI cleanup (1X) to increase total concentration; round 2 elution volume was 20% of round 1 input volume. Template concentration and purity was quantified using NanoDrop 2000 and Qubit dsDNA BR Assays (Thermo Fisher Scientific), and templates were diluted in water to an exact concentration of 2 µg/µl.

SpCas9 RNP preparation. RNPs were produced by complexing a two-component gRNA to SpCas9. In brief, tracrRNA and crRNA were ordered from IDT, suspended in nuclease-free duplex buffer at 100 µM, and stored in single-use aliquots at -80°C. tracrRNA and crRNA were thawed, and 1 µl of each component was mixed 1:1 by volume and annealed by incubation at 37°C for 30 minutes to form a 50 µM gRNA solution in individual aliquots for each electroporation replicate. Recombinant sNLS-SpCas9-sNLS Cas9 (Aldevron, 10 mg/ml, total 0.8 µl) was added to the complexed gRNA at a 1:1 molar ratio and incubated for 15 minutes at 37°C to form an RNP. Individual aliquots of RNPs were incubated for at least 30 seconds at room temperature with HDR templates for each sample prior to electroporation.

Isolation of primary T cells from healthy donors. This study was approved by the Institutional Review Board of the University of Wisconsin-Madison (#2018-0103), and informed consent was obtained from all donors. Peripheral blood was drawn from healthy donors into sterile syringes containing heparin, and transferred to sterile 50 mL conical tubes. Primary human T cells were isolated using negative selection per the manufacturer's instructions (RosetteSep Human T Cell Enrichment Cocktail, STEMCELL Technologies). T cells were counted using a Countess II FL Automated Cell Counter (Thermo Fisher Scientific) with 0.4% Trypan Blue viability stain (Thermo Fisher Scientific). T cells were cultured at a density of 1 million cells/mL in ImmunoCult-XF T cell Expansion Medium (STEMCELL) supplemented with 200 U/mL IL-2 (Peprotech) and stimulated with ImmunoCult Human CD3/CD28/CD2 T cell Activator (STEMCELL) immediately after isolation, per the manufacturer's instructions.

T cell culture. Bulk T cells were cultured in ImmunoCult-XF T cell Expansion Medium at an approximate density of 1 million cells/mL. In brief, T cells were stimulated with ImmunoCult Human CD3/CD28/CD2 T cell Activator (STEMCELL) for 2 days prior to electroporation. On day 3, (24 hours post-electroporation), NV-CAR and NV-mCh T cells were transferred without centrifugation to 1 mL of fresh culture medium (with 500 U/mL IL-2, no activator) and allowed to expand. T cells were passaged, counted, and adjusted to 1 million/mL in fresh medium + IL-2 on days 5 and 7 after isolation. RV-CAR T cells were spinoculated with the RV-CAR construct on day 3 and passaged on day 5 along with the NV-CAR and NV-mCh T cells. Prior to electroporation or spinoculation, the medium was supplemented with 200 U/mL IL-2; post-gene editing, medium was supplemented with 500 U/mL IL-2 (Peprotech).

T cell nucleofection (1 million cell scale). RNPs and HDR templates were electroporated 2 days after T cell isolation and stimulation. During crRNA and tracrRNA incubation, T cells were centrifuged for 3 minutes at 200g and counted using a Countess II FL Automated Cell Counter with 0.4% Trypan Blue viability stain (Thermo Fisher). 1 million cells per replicate were aliquoted into 1.5 mL tubes. During the RNP complexation step (see RNP production), T cell aliquots were centrifuged for 10 min at 90g. During the spin step, 2 µl of HDR template (total 4 µg) per condition were aliquoted to PCR tubes, followed by RNPs (2.8 µl per well; pipette should be set to a higher volume to ensure complete expulsion of viscous solution). Templates and RNPs were incubated at room temperature for at least 30 seconds. After cell centrifugation, supernatants were aspirated, and cells were resuspended in 20 µl P3 buffer (Lonza), then transferred to PCR tubes containing RNP, bringing the total volume per sample to 24 µl. Each sample was transferred directly to a 16 well electroporation cuvette. Typically, no more than 8 reactions were completed at a time to minimize the amount of time T cells spent in P3 buffer. T cells were electroporated with a Lonza 4D Nucleofector with X Unit using pulse code EH115. Immediately after nucleofection, 80 µl of pre-warmed recovery medium with 500 U/mL IL-2 and 25 µl/mL ImmunoCult CD3/CD28/CD2 activator was added to each well of the cuvette. Cuvettes were rested at 37°C in the cell culture incubator for 15 minutes. After 15 minutes, cells were moved to 200 µl total volume of media with IL-2 and activator (see above) in a round bottom 96 well plate.

T cell electroporation (50 million cell scale). RNPs and HDR templates were electroporated 2 days after T cell isolation and stimulation. crRNA and tracrRNA were complexed as described above, using 50 µl of each component (50X scale; 100 µM concentration was maintained). During crRNA and tracrRNA incubation, T cells were centrifuged for 3 minutes at 200g and counted using

a Countess II FL Automated Cell Counter with 0.4% Trypan Blue viability stain (Thermo Fisher). ~50 million cells per replicate were aliquoted per reaction. RNPs were complexed as described above, but with 40 µl Cas9 per reaction (50X scale). During the RNP complexation step, T cell aliquots were centrifuged for 10 min at 90g. During the spin step, 100 µl HDR template (total 200 µg) per condition were aliquoted to 1.5 mL tubes, followed by RNPs (140 µl per well). Templates and RNPs were incubated at room temperature for at least 30 seconds. After cell centrifugation, supernatants were aspirated, and cells were resuspended in 750 µl P3 buffer (Lonza), then transferred to 1.5 mL tubes containing RNP, bringing the total volume per sample to ~1 mL (pellet is assumed to be ~10 µl). Each sample was transferred directly to a 1 mL Nucleocuvette Cartridge (Lonza). T cells were electroporated with a Lonza 4D Nucleofector with LV Unit using pulse code EH115. Immediately after nucleofection, the cartridge was transferred to an incubator to rest at 37°C for 15 minutes. After 15 minutes, cells were removed from the cartridge and seeded in a round bottom 96 well plate, containing 240 µl pre-warmed recovery medium per well (ImmunoCult-XF Medium with 500 U/mL IL-2 and 25 µl/mL ImmunoCult CD3/CD28/CD2 activator). 20 µl of nucleofected cells were added to each well of the 96 well plate, to distribute the recovering cells evenly in small batches. Cells were allowed to recover overnight before transferring the contents of each well to 1 mL fresh medium (ImmunoCult-XF Medium + 500 U/mL IL-2). Cells were counted 3 days after nucleofection, pooled, and cultured according to the same passaging guidelines used for small-scale reactions.

Retrovirus production. CAR retrovirus was manufactured using Phoenix cells (ATCC). In brief, pSFG.iCasp9.2A.14G2A-CD28-OX40-CD3z plasmid was MidiPrepped using the PureYield MidiPrep system (Promega). One day prior to transfection, selected Phoenix cells were plated on

0.01% Poly-L-Lysine coated 15 cm dishes (Sigma Aldrich) at a density of 76,000 cells/cm^2, or ~65% confluency. On transfection day, media was replaced 1 hour prior to transfection of 10 µg pSFG.iCasp9.2A.14G2A-CD28-OX40-CD3z plasmid/plate using iMFectin according to the manufacturer's instructions (GenDEPOT). Media was replaced 18-24 hours later with 10 mL of 50 mM HEPES buffered DMEM + 10% FBS (Gibco). 48 hours later, media was collected, stored at 4°C, and replaced. A second aliquot of media was collected 24 hours later; media aliquots were pooled and centrifuged for 10 min at 2000g to pellet contaminating cells, and supernatants were transferred to a clean conical tube. 1/3 volume Retro-X concentrator (Takara) was added, and supernatants were refrigerated at 4°C for 12-18 hours, then concentrated according to the manufacturer's instructions. Viruses were tested on 3T3 cells prior to use; yields from one 15 cm dish were used for 5 replicate wells of 160,000 T cells per transduction. Viruses were either used immediately for T cell spinoculation or stored at -80°C in single use aliquots.

Retroviral transduction. T cells for RV infection were cultured similarly to NV-CAR and NV-mCh T cells, with two exceptions: 1) T cells were passaged and resuspended without ImmunoCult CD2/CD28/CD3 activator on day 2 post-isolation, and spinoculated on Day 3. RV-CAR T cells returned to the regular passaging schedule on day 5 post-isolation. Prior to spinoculation, non-tissue culture treated 24 well plates were coated with Retronectin according to the manufacturer's instructions (Takara/Clontech). On day 3 post-isolation, T cells were centrifuged at 200 g for 3 minutes, counted, and resuspended to a concentration of 200,000 cells/mL, then stored in the incubator until plates were prepared. Virus was added to retronectin-coated plates in a volume of 400 µl virus in ImmunoCult-XF Medium and centrifuged at 2000g for 2 hours at 32°C. 160,000 T

cells in 800 µl were added to each well and spinoculated at 2000g for 60 minutes at 32°C, brake off. T cells were then transferred to the incubator and left undisturbed for two days.

Flow cytometry and fluorescence-activated cell sorting. CAR was detected using 1A7 anti-14G2a idiotype antibody (gift from Paul Sondel) conjugated to APC with the Lightning-Link APC Antibody Labeling kit (Novus Biologicals). T cells were stained in BD Brilliant Stain Buffer (BD Biosciences). For panels including TCR and CD3, cells were permeabilized and fixed using the BD Cytofix/Cytoperm Plus kit according to the manufacturer's instructions. Flow cytometry was performed on an Attune NxT Flow cytometer (Thermo Fisher Scientific), and fluorescence-activated cell sorting was performed on a FACS Aria (BD). T cells from Donors 1 and 2 were stained and analyzed on day 9 of manufacture using fresh cells. For donors 3 and 4, only TCR, CAR, and CD62L were measured on day 9 of manufacture. The change in protocol was made due to equipment restrictions related to institutional COVID-19 biosafety precautions, and CD62L was selected for analysis due to the known effects of cryopreservation on expression levels[67].

In-Out PCR. Genomic DNA was extracted from 100,000 cells per condition using DNA QuickExtract (Lucigen), and incubated at 65°C for 15 min, 68°C for 15 min, and 98°C for 10 min. Genomic integration of the CAR was confirmed by In-out PCR using a forward primer upstream of the *TRAC* left homology arm, and a reverse primer binding within the CAR sequence. Primer sequences are listed in **Supplementary Table 6**. PCR was performed according to the manufacturer's instructions using Q5 Hot Start Polymerase (NEB) using the following program: 98°C (30 s), 35 cycles of 98°C (10 s), 62°C (20 s), 72°C (2 min), and a final extension at 72°C (2 min).

Next Generation Sequencing of genomic DNA. Indel formation at the *TRAC* locus was measured using Next Generation Sequencing (Illumina). Genomic PCR was performed according to the manufacturer's instructions using Q5 Hot Start polymerase (NEB); primers are listed in **Supplementary Table 6**. Products were purified using SPRI cleanup with AMPure XP beads (Beckman Coulter), and sequencing indices were added with a second round of PCR using indexing primers (Illumina), followed by a second SPRI cleanup. Samples were pooled and sequenced on an Illumina MiniSeq according to the manufacturer's instructions. Analysis was performed using CRISPR RGEN (rgenome.net).

Genome-wide, off-target analysis. Genomic DNA from human primary $CD4^+/CD8^+$ T cells was isolated using Gentra Puregene Kit (Qiagen) according to the manufacturer's instructions. CHANGE-seq was performed as previously described[23]. Briefly, purified genomic DNA was tagmented with a custom Tn5-transposome to an average length of 400 bp, followed by gap repair with Kapa HiFi HotStart Uracil+ DNA Polymerase (KAPA Biosystems) and Taq DNA ligase (NEB). Gap-repaired tagmented DNA was treated with USER enzyme (NEB) and T4 polynucleotide kinase (NEB). Intramolecular circularization of the DNA was performed with T4 DNA ligase (NEB) and residual linear DNA was degraded by a cocktail of exonucleases containing Plasmid-Safe ATP-dependent DNase (Lucigen), Lambda exonuclease (NEB) and Exonuclease I (NEB). *In vitro* cleavage reactions were performed with 125 ng of exonuclease-treated circularized DNA, 90 nM of SpCas9 protein (NEB), NEB buffer 3.1 (NEB) and 270 nM of sgRNA, in a 50 µL volume. Cleaved products were A-tailed, ligated with a hairpin adaptor (NEB), treated with USER enzyme (NEB) and amplified by PCR with barcoded universal primers

NEBNext Multiplex Oligos for Illumina (NEB), using Kapa HiFi Polymerase (KAPA Biosystems). Libraries were quantified by qPCR (KAPA Biosystems) and sequenced with 151 bp paired-end reads on an Illumina NextSeq instrument. CHANGE-seq data analyses were performed using open-source CHANGE-seq analysis software (https://github.com/tsailabSJ/changeseq).

Cytokine Analysis. Cytokine analysis was performed using a V-PLEX Proinflammatory Panel 1 Human Kit (Meso Scale Discovery, Catalog No K15049D-2) according to the manufacturer's protocol. The following cytokines were measured: IFNγ, IL-1β, IL-2, IL-4, IL-6, IL-8, IL-10, IL-12p70, IL-13, and TNF-α. In brief, media was collected from the final day of cell culture before injection into mice and flash frozen and stored at -80°C. For co-culture samples, 250,000 T cells were co-cultured with 50,000 cancer cells in 250 µl ImmunoCult XF T cell expansion medium for 24 hours prior to media collection. On the day of the assay, media was thawed and 50 µl of media was used to perform all measurements in duplicate. Figures were produced using GraphPad PRISM 8. Data were normalized by calculating cytokine production per cell based on the total concentration of cells calculated at media collection.

Immunoblotting. Equivalent number of T cells (1x10e6) were lysed in Laemmli Sample Buffer with β-mercaptoethanol (Bio-Rad, CA). Total cell lysate for each sample were resolved on 12% SDS-PAGE gels and transferred to polyvinylidene fluoride membranes (Millipore, Billerica, MA). The membranes were blocked in LI-COR blocking buffer (LI-COR, NE), Immunoblotting was performed by incubating the membranes with anti-human CD247 (Mouse. BD Biosciences), anti-human CD247 $pTyr^{142}$ (Mouse, BD Biosciences), and anti-human GAPDH (Rabbit. Cell Signaling Tech, MA), according to the manufacturer's recommendations. The membranes were

then washed with TBST and incubated with fluorescent secondary antibodies (LI-COR, NE) and the immunoreactive bands were visualized using Odyssey ® CLx imaging system (LI-COR, NE).

***In Vitro* Cytotoxicity Assays.** *For **Fig. 6c**:* 10,000 AkaLUC-GFP CHLA20 cells were seeded in triplicate per condition in a 96 well flat bottom plate. 48 hours later, 50,000 T cells were added to each well. 1 µl (0.05 µg) of CF® 594 Annexin V antibody (Biotium) was added to the wells. The plate was centrifuged at 100g for 1 minute and then placed in The IncuCyte® S3 Live-Cell Analysis System (Sartorius, Catalog No 4647), stored at 37°C, 5% CO_2. Images were taken every 2 hours for 48 hours. Green object count was used to calculate the number of cancer cells in each well. Red object count was used to calculate the number of objects staining positive for Annexin V, an early apoptosis marker. Fluorescent images were analyzed with IncuCyte Base Analysis Software. *For **Fig. 6b**:* 10,000 AkaLUC-GFP CHLA20 cells or 10,000 H2B-mCherry M21 cells were seeded in triplicate per condition in a 96 well flat bottom plate. 24 hours later, 50,000 T cells were added to each well. The 96 well plate was placed in a live cell imaging chamber at 37°C and 5% CO_2 and imaged on a Nikon Epifluorescent scope, with images taken every 12 hours for 48 hours. The change in protocol was made due to institutional COVID-19 biosafety precautions.

Single cell RNA sequencing. 24 hours prior to assay, 200,000 AkaLUC-CHLA20 cells were plated in 12 well plates and cultured overnight. One week after electroporation (day 9 post-isolation), T cells were counted and pooled into a single bank for characterization studies (scRNA-seq, IncuCyte cytotoxicity assay and *in vivo* experiments). Media was aspirated from cancer cells, and 1 million T cells in ImmunoCult-XF Medium + 500 U/mL IL-2 were seeded on the cancer cells, then cultured for 24 hours. A parallel T cell-only single culture (termed “pre-antigen”) was

set up at the same density in a separate 12 well plate. The next day, co-culture cells were trypsinized for donor 1 and washed off the plate with media, and cells were singularized with a 35 μM cell strainer (Corning). For donor 2, co-culture cells were stained for CD45 and CAR, and FACS sorted into $CD45^{+}CAR^{+}$ and $CD45^{+}CAR^{-}$ fractions prior to sample submission. Cells were counted with a Countess II FL cell counter using trypan blue exclusion (Thermo Fisher Scientific), and samples were prepared for single cell RNA sequencing with the 10X Genomics 3' kit (v3 chemistry) according to the manufacturer's instructions. Libraries were sequenced using the Illumina NovaSeq 6000 system. FASTQ files were aligned with Cellranger v3.0.1 to custom reference genomes that included added sequences for the transgene(s) used in each culture condition (e.g., the *TRAC* NV-CAR donor sequence, mCherry donor sequence, etc.). Downstream analyses were performed using Seurat 3. In brief, each dataset was filtered to include only cells with 200 or more unique genes, and genes expressed in three or more cells. Data were normalized and scaled, and mitochondrial mapping percentage was regressed out as a confounding source of variation. Datasets were then integrated, and dimensionality reduction was performed with Principal Components Analysis. Cells were clustered based on their genome-wide transcriptional profiles using t-distributed stochastic neighbor embedding (tSNE), and differential gene expression was calculated using Seurat 3. Clusters were For each sample, cells expressing the transgene of interest (CAR or mCherry) were identified, and transgene-negative cells were removed from the dataset. All analysis scripts will be deposited in the Saha Lab GitHub repository upon publication.

***In vivo* human neuroblastoma xenograft mouse model.** All animal experiments were approved by the University of Wisconsin-Madison Animal Care and Use Committee (ACUC). Male and

female NSG mice (9-25 weeks old) were subcutaneously injected with 10 million AkaLUC-GFP CHLA20 human neuroblastoma cells in the side flank to establish tumors. Six days later (Day 0), established tumors were verified by bioluminescence with the PerkinElmer *In Vivo* Imaging System (IVIS), and 10 million T cells were injected through the tail vein into each mouse. Mice were followed for weight loss and overall survival. On imaging days, mice were sedated using isoflurane and received intraperitoneal injections of ~120 mg/kg D-luciferin (GoldBio). Fifteen minutes later, mice were imaged via IVIS. Imaging was repeated every 3 to 4 days, starting 1 day before initial T cell injection (Day -1). Mice were injected with 100,000 IU of human IL-2 subcutaneously on day 0, day 4, and with each subsequent IVIS reading. In order to quantify the total flux in the IVIS images, a region of interest (ROI) was drawn around the bottom half of each mouse with the total flux being calculated by Living Image® software (PerkinElmer; Total flux = the radiance (photons/sec) in each pixel summed or integrated over the ROI area (cm^2) x 4π). The absolute minimum total flux value was subtracted from each image to minimize background signal. For donors 1, 3, and 4, mice were maintained until tumors reached 20mm in any dimension by digital caliper as defined by the ACUC.

Flow cytometric analysis of splenic and tumor-infiltrating T cells. For donor 2, all mice were euthanized on day 25. Tumors and spleens were removed, mechanically dissociated, and passed through a Corning® 35µm cell strainer. Cell suspensions were centrifuged at 300g for 10 minutes, and then digested with ACK lysing buffer (Lonza). The cells were then washed and centrifuged at 300g for 10 minutes, and then resuspended in 10 ml PBS, 10 µl of which was added to 10 ml of ISOTON® diluent and counted on the COULTER COUNTER® Z1 Series Particle Counter (Beckman Coulter). From this count, $1x10^6$ cells were added to flow cytometry tubes in staining

buffer (PBS with 2% FBS) and stained with antibodies for hCD45, mCD45, scFV 14G2a CAR, and PD-1 (see **Supplementary Table 5 for antibody information**). The cells were then washed with PBS, centrifuged at 300g for 10 minutes, and 0.5ul of Ghost Dye™ Red 780 viability dye (Tonbo Biosciences) was added for 20 minutes at room temperature. Cells were then washed with staining buffer, spun down, and resuspended in 400 µl of staining buffer. Cells were then run on an Attune™ NXT flow cytometer (Thermo Fisher Scientific). Subsequent analysis was performed using Flowjo™ software (BD). For donors 3 and 4, spleens and tumors were analyzed as mice reached euthanasia criteria.

Statistical analysis. Unless otherwise specified, all analyses were performed using GraphPad Prism (v.8.0.1), and error bars represent mean ± SD; ns = $p>=0.05$, * for $p<0.05$, ** for $p<0.01$, *** for $p<0.001$,**** for $p<0.0001$. For Fig. 2b, error bars show SEM. Statistical analyses for cytokine data were performed using a two-tailed Mann-Whitney test in GraphPad Prism. All box plots show median (horizontal line), interquartile range (hinges), and smallest and largest values (whiskers). Statistical significance for differential gene expression was determined with Seurat 3 using the non-parametric Wilcoxon rank sum test. Statistical significance for **Fig. 7c** was calculated using the Mantel-Cox Test.

Data Availability. The data that support the findings of this study will be made available in the public domain upon publication.

Data Reporting. The Reporting Summary document includes information about the statistics, software, data, and sample preparation methods used for this study. For *in vivo* experiments,

established tumor burden was verified by IVIS luciferase imaging prior to infusion. Mice were arranged according to tumor burden and distributed evenly across conditions. The experiments were not randomized and the investigators were not blinded during experiments and outcome assessment.

Acknowledgments: We thank members of the Saha and Capitini labs and John Hosmer-Quint for helpful discussion and comments on the manuscript, the University of Wisconsin (UW) Carbone Cancer Center Flow Cytometry Laboratory for assistance with flow cytometry experiments, and Aldevron for technical support with Cas9 proteins. We thank Tyler Duellman and the University of Wisconsin-Madison Biotechnology Center Gene Expression Center the DNA Sequencing Facility for providing single nuclei library preparation and next generation sequencing services. We thank Malcolm Brenner (Baylor College of Medicine) for sharing of the RV-CAR plasmid, Paul Sondel and the National Cancer Institute for 1A7 anti-CAR antibody, James Thomson and Jue Zhang (Morgridge Institute for Research) for the AkaLUC-GFP CHLA20 cancer line used for *in vivo* studies, and Sushmita Roy, Sunnie Grace McCalla, Madeline Smerchansky and Kurt Mueller for helpful discussions and assistance with scRNA-seq analysis. We thank Madeline Smerchansky and Dan Cappabianca for assistance with scale up experiments. We acknowledge generous support from the National Science Foundation CBET-1645123 (CMC and KS), EEC-1648035 (KS), AWD-101645-G3/RJ375-G3 (KS), and NSF Graduate Research Fellowship Program DGE-1747503, to K.P.M and N.J.P.); National Institutes of Health/National Cancer Institute R01 CA215461 (CMC), National Institute of General Medical Sciences R35 GM119644-01 (KS), Biotechnology Training Program T32GM008349 (K.P.M); University of Wisconsin Carbone Cancer Center Support Grant P30 CA014520 Cell Based Immunotherapy Supplement

(CMC and KS); St. Baldrick's – Stand up to Cancer Pediatric Dream Team Translational Research Grant SU2C-AACR-DT-27-17 (CMC); American Cancer Society Research Scholar grant RSG-18-104-01-LIB (CMC); and the MACC Fund (CMC). Stand Up to Cancer is a division of the Entertainment Industry Foundation. Research grants are administered by the American Association for Cancer Research, the Scientific Partner of SU2C. The contents of this article do not necessarily reflect the views or policies of the Department of Health and Human Services, nor does mention of trade names, commercial products, or organizations imply endorsement by the US Government.

Authors' contributions: These authors contributed equally: K.P.M. and N.J.P. K.P.M. and L.A.S. designed and cloned the NV-CAR and NV-mCh plasmids. K.P.M. and N.J.P. isolated and cultured T cells and performed nonviral transfections. K.P.M. and A.D. performed viral transductions. K.P.M. and B.R. performed and analyzed scRNA-seq experiments. M.F., L.A.S., and A.D. performed flow cytometry. N.J.P. and B.R. performed and analyzed NGS experiments. N.J.P and M.F. performed cytokine experiments and N.J.P. analyzed cytokine data. M.F. conducted *in vivo* experiments. K.P.M., N.J.P. and A.A. performed *in vitro* co-cultures. C.L. performed the CHANGE-seq assay. K.P.M. and N.J.P. wrote the manuscript with input from all authors. S.T., K.S. and C.M.C. supervised the research. K.P.M., N.J.P., M.F., L.A.S., C.L., A.D., A.A., and B.R. performed experiments and analyzed the data.

Conflicts of interest: K.P.M., N.J.P., M.H.F., L.A.S., A.D., C.M.C. and K.S. are inventors on a patent application related to this manuscript. No other conflicts of interest are reported.

References

1. Goff, S. L. *et al.* Pilot Trial of Adoptive Transfer of Chimeric Antigen Receptor-transduced T Cells Targeting EGFRvIII in Patients With Glioblastoma. *J. Immunother.* **42**, 126–135 (2019).
2. O'Rourke, D. M. *et al.* A single dose of peripherally infused EGFRvIII-directed CAR T cells mediates antigen loss and induces adaptive resistance in patients with recurrent glioblastoma. *Sci. Transl. Med.* **9**, (2017).
3. Kahlon, K. S. *et al.* Specific recognition and killing of glioblastoma multiforme by interleukin 13-zetakine redirected cytolytic T cells. *Cancer Res.* **64**, 9160–9166 (2004).
4. Newick, K., Moon, E. & Albelda, S. M. Chimeric antigen receptor T-cell therapy for solid tumors. *Mol Ther Oncolytics* **3**, 16006 (2016).
5. RodrÍguez, E., Schetters, S. T. T. & van Kooyk, Y. The tumour glyco-code as a novel immune checkpoint for immunotherapy. *Nat. Rev. Immunol.* **18**, 204–211 (2018).
6. Fesnak, A. D., June, C. H. & Levine, B. L. Engineered T cells: the promise and challenges of cancer immunotherapy. *Nat. Rev. Cancer* **16**, 566–581 (2016).
7. Piscopo, N. J. *et al.* Bioengineering Solutions for Manufacturing Challenges in CAR T Cells. *Biotechnol. J.* **13**, (2018).
8. Wang, X. & Rivière, I. Clinical manufacturing of CAR T cells: foundation of a promising therapy. *Mol Ther Oncolytics* **3**, 16015 (2016).
9. Nobles, C. L. *et al.* CD19-targeting CAR T cell immunotherapy outcomes correlate with genomic modification by vector integration. *J. Clin. Invest.* **130**, 673–685 (2020).
10. van der Loo, J. C. M. & Wright, J. F. Progress and challenges in viral vector manufacturing. *Hum. Mol. Genet.* **25**, R42-52 (2016).

11. Monjezi, R. *et al.* Enhanced CAR T-cell engineering using non-viral Sleeping Beauty transposition from minicircle vectors. *Leukemia* **31**, 186–194 (2017).

12. Foster, J. B. *et al.* Purification of mRNA Encoding Chimeric Antigen Receptor Is Critical for Generation of a Robust T-Cell Response. *Hum. Gene Ther.* **30**, 168–178 (2019).

13. Jinek, M. *et al.* A programmable dual-RNA-guided DNA endonuclease in adaptive bacterial immunity. *Science* **337**, 816–821 (2012).

14. McGuire, A. L. *et al.* The road ahead in genetics and genomics. *Nat. Rev. Genet.* **21**, 581–596 (2020).

15. Doudna, J. A. The promise and challenge of therapeutic genome editing. *Nature* **578**, 229–236 (2020).

16. Eyquem, J. *et al.* Targeting a CAR to the TRAC locus with CRISPR/Cas9 enhances tumour rejection. *Nature* **543**, 113–117 (2017).

17. Sachdeva, M. *et al.* Repurposing endogenous immune pathways to tailor and control chimeric antigen receptor T cell functionality. *Nat. Commun.* **10**, 5100 (2019).

18. Fraietta, J. A. *et al.* Determinants of response and resistance to CD19 chimeric antigen receptor (CAR) T cell therapy of chronic lymphocytic leukemia. *Nat. Med.* **24**, 563–571 (2018).

19. Gardner, R. A. *et al.* Intent-to-treat leukemia remission by CD19 CAR T cells of defined formulation and dose in children and young adults. *Blood* **129**, 3322–3331 (2017).

20. Feucht, J. *et al.* Calibration of CAR activation potential directs alternative T cell fates and therapeutic potency. *Nat. Med.* **25**, 82–88 (2019).

21. Kalos, M. *et al.* T cells with chimeric antigen receptors have potent antitumor effects and can establish memory in patients with advanced leukemia. *Sci. Transl. Med.* **3**, 95ra73 (2011).

22. Xu, Y. *et al.* Closely related T-memory stem cells correlate with in vivo expansion of CAR.CD19-T cells and are preserved by IL-7 and IL-15. *Blood* **123**, 3750–3759 (2014).

23. Zah, E. *et al.* Systematically optimized BCMA/CS1 bispecific CAR-T cells robustly control heterogeneous multiple myeloma. *Nat. Commun.* **11**, 2283 (2020).

24. Shah, N. N. & Fry, T. J. Mechanisms of resistance to CAR T cell therapy. *Nat. Rev. Clin. Oncol.* **16**, 372–385 (2019).

25. Lynn, R. C. *et al.* c-Jun overexpression in CAR T cells induces exhaustion resistance. *Nature* **576**, 293–300 (2019).

26. Louis, C. U. *et al.* Antitumor activity and long-term fate of chimeric antigen receptor-positive T cells in patients with neuroblastoma. *Blood* **118**, 6050–6056 (2011).

27. Hanlon, K. S. *et al.* High levels of AAV vector integration into CRISPR-induced DNA breaks. *Nat. Commun.* **10**, 4439 (2019).

28. Roth, T. L. *et al.* Reprogramming human T cell function and specificity with non-viral genome targeting. *Nature* **559**, 405–409 (2018).

29. Kath, J. *et al.* Fast, efficient and virus-free generation of TRAC-replaced CAR T cells. *bioRxiv* 2021.02.14.431017 (2021) doi:10.1101/2021.02.14.431017.

30. Roth, T. L. *et al.* Pooled Knockin Targeting for Genome Engineering of Cellular Immunotherapies. *Cell* **181**, 728-744.e21 (2020).

31. Mueller, K., Carlson-Stevermer, J. & Saha, K. Increasing the precision of gene editing in vitro, ex vivo, and in vivo. *Curr Opin Biomed Eng* **7**, 83–90 (2018).

32. Pulè, M. A. *et al.* A chimeric T cell antigen receptor that augments cytokine release and supports clonal expansion of primary human T cells. *Mol. Ther.* **12**, 933–941 (2005).

33. Goodwin, M. *et al.* CRISPR-based gene editing enables FOXP3 gene repair in IPEX patient cells. *Science Advances* **6**, (2020).

34. Lazzarotto, C. R. *et al.* CHANGE-seq reveals genetic and epigenetic effects on CRISPR-Cas9 genome-wide activity. *Nat. Biotechnol.* (2020) doi:10.1038/s41587-020-0555-7.

35. Long, A. H. *et al.* 4-1BB costimulation ameliorates T cell exhaustion induced by tonic signaling of chimeric antigen receptors. *Nat. Med.* **21**, 581–590 (2015).

36. Gomes-Silva, D. *et al.* Tonic 4-1BB Costimulation in Chimeric Antigen Receptors Impedes T Cell Survival and Is Vector-Dependent. *Cell Rep.* **21**, 17–26 (2017).

37. Ajina, A. & Maher, J. Strategies to Address Chimeric Antigen Receptor Tonic Signaling. *Mol. Cancer Ther.* **17**, 1795–1815 (2018).

38. Pule, M. A. *et al.* Virus-specific T cells engineered to coexpress tumor-specific receptors: persistence and antitumor activity in individuals with neuroblastoma. *Nat. Med.* **14**, 1264–1270 (2008).

39. Heczey, A. *et al.* CAR T cells administered in combination with lymphodepletion and PD-1 inhibition to patients with neuroblastoma. *Mol. Ther.* **25**, 2214–2224 (2017).

40. Hong, M., Clubb, J. D. & Chen, Y. Y. Engineering CAR-T Cells for Next-Generation Cancer Therapy. *Cancer Cell* (2020) doi:10.1016/j.ccell.2020.07.005.

41. Martinez, M. & Moon, E. K. CAR T Cells for Solid Tumors: New Strategies for Finding, Infiltrating, and Surviving in the Tumor Microenvironment. *Front. Immunol.* **10**, 128 (2019).

42. Tokarew, N., Ogonek, J., Endres, S., von Bergwelt-Baildon, M. & Kobold, S. Teaching an old dog new tricks: next-generation CAR T cells. *Br. J. Cancer* **120**, 26–37 (2019).

43. Tanna, J. G., Ulrey, R., Williams, K. M. & Hanley, P. J. Critical testing and parameters for consideration when manufacturing and evaluating tumor-associated antigen-specific T cells. *Cytotherapy* **21**, 278–288 (2019).

44. Shin, J. J. *et al.* Controlled Cycling and Quiescence Enables Efficient HDR in Engraftment-Enriched Adult Hematopoietic Stem and Progenitor Cells. *Cell Rep.* **32**, 108093 (2020).

45. Nguyen, D. N. *et al.* Polymer-stabilized Cas9 nanoparticles and modified repair templates increase genome editing efficiency. *Nat. Biotechnol.* **38**, 44–49 (2020).

46. Kunz, A. *et al.* Optimized Assessment of qPCR-Based Vector Copy Numbers as a Safety Parameter for GMP-Grade CAR T Cells and Monitoring of Frequency in Patients. *Mol Ther Methods Clin Dev* **17**, 448–454 (2020).

47. Lu, A. *et al.* Application of droplet digital PCR for the detection of vector copy number in clinical CAR/TCR T cell products. *J. Transl. Med.* **18**, 191 (2020).

48. Nelson, C. E. *et al.* Long-term evaluation of AAV-CRISPR genome editing for Duchenne muscular dystrophy. *Nat. Med.* **25**, 427–432 (2019).

49. Webber, B. R. *et al.* Highly efficient multiplex human T cell engineering without double-strand breaks using Cas9 base editors. *Nat. Commun.* **10**, 5222 (2019).

50. Dai, X. *et al.* One-step generation of modular CAR-T cells with AAV-Cpf1. *Nat. Methods* **16**, 247–254 (2019).

51. Ren, J. *et al.* A versatile system for rapid multiplex genome-edited CAR T cell generation. *Oncotarget* **8**, 17002–17011 (2017).

52. Khajanchi, N. & Saha, K. Controlling CRISPR with Small Molecule Regulation for Somatic Cell Genome Editing. *Mol. Ther.* (2021) doi:10.1016/j.ymthe.2021.06.014.

53. Maeda, T. *et al.* Regeneration of CD8αβ T Cells from T-cell-Derived iPSC Imparts Potent Tumor Antigen-Specific Cytotoxicity. *Cancer Res.* **76**, 6839–6850 (2016).

54. Nagano, S. *et al.* High Frequency Production of T Cell-Derived iPSC Clones Capable of Generating Potent Cytotoxic T Cells. *Mol Ther Methods Clin Dev* **16**, 126–135 (2020).

55. Themeli, M. *et al.* Generation of tumor-targeted human T lymphocytes from induced pluripotent stem cells for cancer therapy. *Nat. Biotechnol.* **31**, 928–933 (2013).

56. Shukla, S. *et al.* Progenitor T-cell differentiation from hematopoietic stem cells using Delta-like-4 and VCAM-1. *Nat. Methods* **14**, 531–538 (2017).

57. Liu, E. *et al.* Cord blood NK cells engineered to express IL-15 and a CD19-targeted CAR show long-term persistence and potent antitumor activity. *Leukemia* **32**, 520–531 (2018).

58. Terakura, S. *et al.* Generation of CD19-chimeric antigen receptor modified CD8+ T cells derived from virus-specific central memory T cells. *Blood* **119**, 72–82 (2012).

59. Cromer, M. K. *et al.* Global Transcriptional Response to CRISPR/Cas9-AAV6-Based Genome Editing in CD34+ Hematopoietic Stem and Progenitor Cells. *Mol. Ther.* **26**, 2431–2442 (2018).

60. Viaud, S. *et al.* Switchable control over in vivo CAR T expansion, B cell depletion, and induction of memory. *Proc. Natl. Acad. Sci. U. S. A.* **115**, E10898–E10906 (2018).

61. Hwang, J.-R., Byeon, Y., Kim, D. & Park, S.-G. Recent insights of T cell receptor-mediated signaling pathways for T cell activation and development. *Exp. Mol. Med.* **52**, 750–761 (2020).

62. Wang, K. *et al.* A multiscale simulation framework for the manufacturing facility and supply chain of autologous cell therapies. *Cytotherapy* **21**, 1081–1093 (2019).

63. Lesueur, L. L., Mir, L. M. & André, F. M. Overcoming the Specific Toxicity of Large Plasmids Electrotransfer in Primary Cells In Vitro. *Mol. Ther. Nucleic Acids* **5**, e291 (2016).

64. Ruella, M. *et al.* Induction of resistance to chimeric antigen receptor T cell therapy by transduction of a single leukemic B cell. *Nat. Med.* **24**, 1499–1503 (2018).

65. Clement, K., Hsu, J. Y., Canver, M. C., Joung, J. K. & Pinello, L. Technologies and Computational Analysis Strategies for CRISPR Applications. *Mol. Cell* **79**, 11–29 (2020).

66. Vakulskas, C. A. *et al.* A high-fidelity Cas9 mutant delivered as a ribonucleoprotein complex enables efficient gene editing in human hematopoietic stem and progenitor cells. *Nat. Med.* **24**, 1216–1224 (2018).

67. Costantini, A. *et al.* Effects of cryopreservation on lymphocyte immunophenotype and function. *J. Immunol. Methods* **278**, 145–155 (2003).

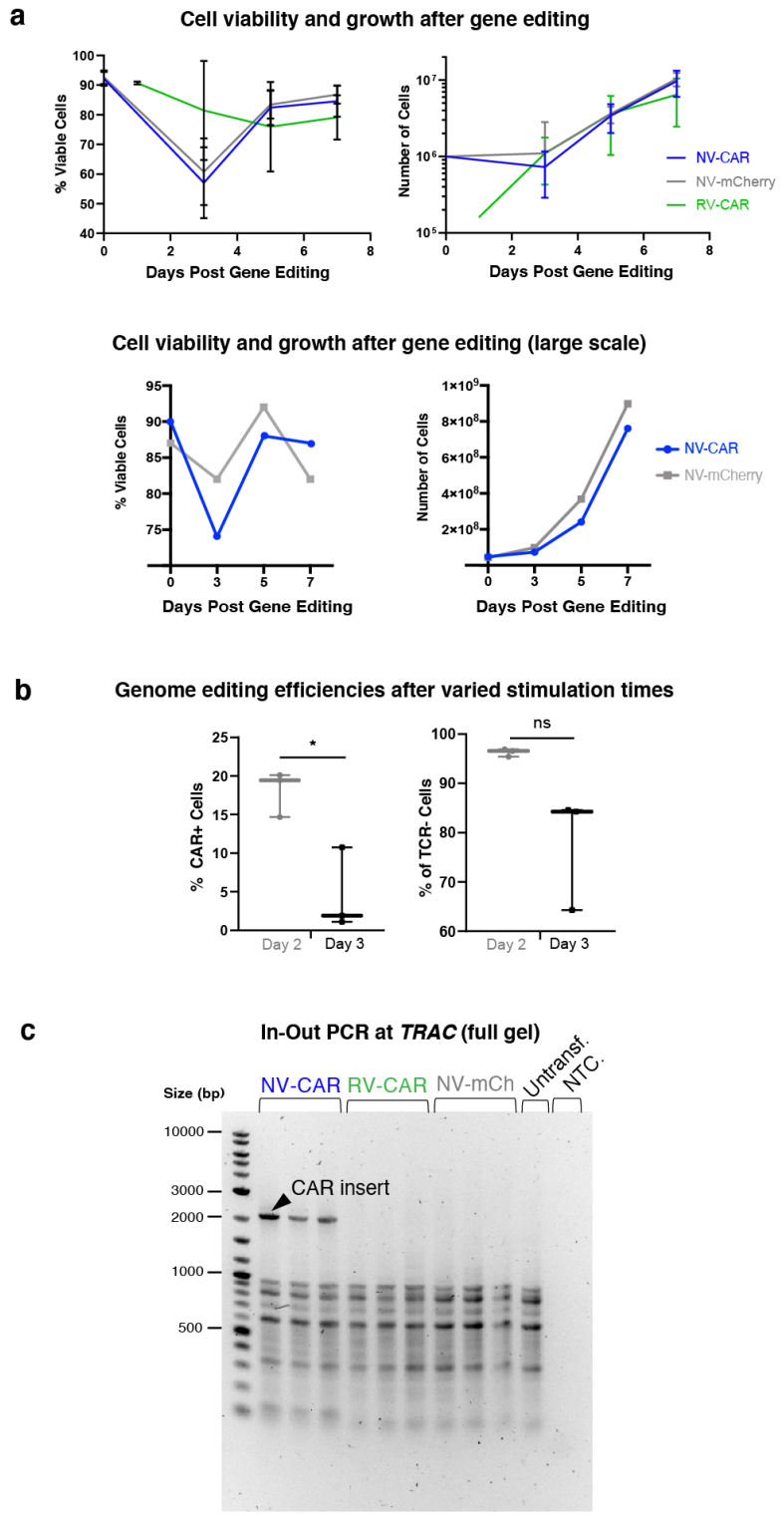

Extended Data Figure 1. Characterization of T cell products during manufacturing. a, Top left, Viability of cells throughout the manufacturing timeline, pooled for all 4 donors. **Top right,** Cell counts throughout the manufacture calendar, pooled for all 4 donors. NV-CAR (blue) N=36;

RV-CAR (green) N=27; NV-mCh (gray) N=25. **Bottom left,** Viability of cells throughout the manufacturing timeline with 50 million cells (1 mL size reactions), using the 4D-Nucleofector LV unit for gene editing scaleup (Lonza). **Bottom right,** Cell counts throughout the manufacture calendar, using the 4D-Nucleofector LV unit for gene editing scaleup. N=1 for each reaction. **b, Left**, Percent of CAR+ cells as measured by flow cytometry when electroporated on day 2 or day 3 post-isolation. **Right**, Percent of TCR- cells as measured by flow cytometry when electroporated on day 2 or day 3 post-isolation. **c,** In-out PCR confirming NV-CAR insertion, full gel from **Fig. 2a** shown. PCR was optimized to minimize off-target amplification which occurs only for fragments <1 kb across the genome and does not vary by sample. N=3 for all samples from one donor. Untransf., donor-matched untransfected control T cells; NTC = non-template control. * indicates p<=0.05.

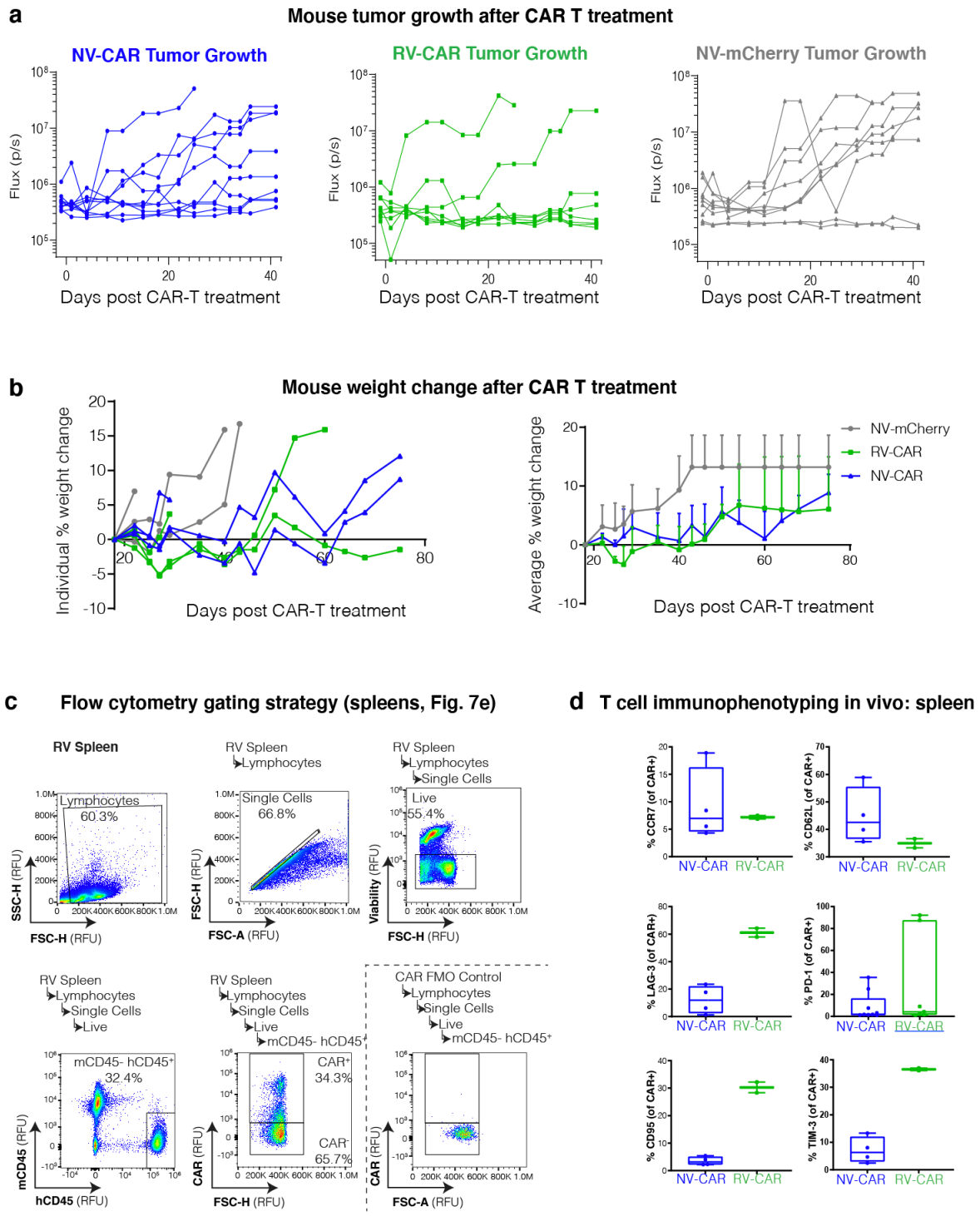

Extended Data Figure 2. Bioluminescence, tumor growth, weight gains, and T cell persistence and exhaustion after T cell treatment *in vivo*. a, Flux measurements for individual luciferase-positive tumors for all mouse experiments. NV-CAR, N=10. RV-CAR, N=8. NV-mCh, N=7. **b, Left**, individual mouse percent weight change throughout the experiment. **Right**, average

percent weight change in mice per treatment condition. **c,** Flow cytometric gating strategy used to assay mouse spleens for human T cells and CAR-positive cells. **d,** Boxplots showing the expression levels of subtype and exhaustion markers on human T cells found in mouse spleens.